Volume 4 JANUARY, 1933 Number 1

PHYSICS

A Journal of General and Applied Physics

The Diffusion of Thorium in Tungsten

GORTON R. FONDA, ANDREW H. YOUNG AND AMY WALKER, *Research Laboratory, General Electric Company, Schenectady*

(Received October 20, 1932)

Thoriated tungsten wires have been so heat-treated in gas as to develop variations in grain size, ranging in length from 4 μ to 3 cm. These variations produced marked changes in the thermionic emissive characteristics, such as rates of deactivation and of activation and duration of emissive life at normal operating temperature. The heat of diffusion remained unaffected. It was concluded that intergranular diffusion of thorium through tungsten is relatively too rapid to be measured and that the observed phenomenon depends purely on intragranular diffusion. This conception is in accord with the existence of a critical grain size for the realization of a maximum emissive life. Experiments are also described to demonstrate the spreading of thorium atoms over the surface of a single crystal of tungsten and to manifest the effect of slight strains in the lattice upon activation.

EXAMINATION of diverse lots of thoriated tungsten wires has shown that the values of the diffusion and activation constants may vary widely from the values cited by Langmuir.[1] These apparent discrepancies were finally found to be related to grain size and their explanation in that light has furnished fresh experimental evidence on the mechanism of diffusion of one metal within another, which is a development of the conception of Compton and Langmuir[2] that "diffusion is particularly rapid along crystal grain boundaries but must occur also from the interior of crystals to these boundaries and probably also through the surface layer of crystals."

The clue to this relationship, as well as the elimination of other possible causes, came from a study of the variation in emissive life, expressed as the length of time for the emission of a filament 0.010 cm in diameter to drop to 20 percent of its initial value at a temperature of 2000°K. The construction of the kenotron and the general technique followed in all tests were the same as those described by Dushman, Rowe, Ewald and Kidner.[3] The life was found to be uniform for different filaments cut from the same wire lot. Seven different wire lots examined exhibited, however, a range in life varying from 140 to 1200 hours. Chemical analysis showed variations in thoria content of the various lots ranging from 0.9 percent to 2.8 percent but these were unrelated to length of life. It was found, furthermore, that the loss of thoria during life amounted to less than 10 percent for both the good and poor wires. The size of the thoria particles was found to vary somewhat but this also was unrelated to life.

It then developed that the controlling factor lay in the heat treatment which the wire received, and that the effectiveness of this lay in the possibility of thereby increasing the grain size to a critical value. The life of a 200 hour wire, for instance, was increased seven-fold by a 1 min. flash at 3000°K in argon at 60 cm pressure. An incidental result of this is an increase in the concentration of reduced thorium by reason of the effect of a heavy gas in retarding the evaporation of a metal. The resistivity of thoriated

[1] I. Langmuir, Phys. Rev. **22**, 357 (1923).

[2] K. T. Compton and I. Langmuir, Rev. Mod. Phys. **2**, 138 (1930).

[3] S. Dushman, H. N. Rowe, J. Ewald and C. A. Kidner, Phys. Rev. **25**, 338 (1925).

wires which had been tested in 50 cm pressure of argon rose from the normal value for pure tungsten of 5.5 $(10)^{-6}$ ohms per cm^3 to 5.8 $(10)^{-6}$, denoting the liberation of thorium and its entrance into solid solution with the tungsten. Such a change was absent in vacuum. This could have been only of minor importance upon life, however, for a wire made from a powdered mixture of tungsten with 1 percent of metallic thorium showed the abnormally short life of 90 hours under normal treatment despite the fact that its temperature coefficient of resistance was 20 percent below normal, demonstrating the retention of a large amount of metallic thorium in solid solution. The high temperature flash in argon had the same effect of increasing the grain size of this wire and this was accompanied by the same abnormal increase in life. Furthermore, the same favorable result came from a high temperature treatment in hydrogen, too light a gas to retard appreciably the evaporation of thorium. In vacuum the treatment gave only a slight improvement and in turn there was a greater resistance to grain growth. Even under the normal treatment a continuous improvement in life resulted during successive life tests, each preceded by the customary activation and accompanied by a slight but continuous increase in grain size.

Similar effects on grain size have been observed by Jeffries.[4] He has described the slight grain growth that occurs on long continued burning at low temperatures and has explained the effect of thoria in producing exaggerated grain growth when a wire is flashed on abruptly at temperatures above 2800°K. It was found possible by variations in this treatment to vary the grain size at will up to single crystals several cm long.

The behavior of such wires with respect to emissive characteristics is described below. From these it developed that the fundamental phenomenon involved is one of intragranular diffusion. Its relation to grain size was found to explain the variations in life.

Deactivation

An extended study was made of the deactivation characteristics of different wires. The conventional method was followed—first flashing the filament for 3 minutes at 2800°K to form a supply of reduced thorium and then deactivating at the temperature in question. The course of the deactivation curve was found by interrupting this process at intervals and measuring the emission at 1450°K, a temperature so low that the status of the thorium with respect to diffusion and to evaporation was maintained unchanged.

The diffusion coefficient, D, was calculated from the latter portion of the curve according to the second method employed by Langmuir,[1] involving the equation

$$D=\frac{\Delta \log\,(1/(1-\theta)-1/(1-\theta_r))}{\Delta t}\,\frac{R^2 2.303}{5.783},$$

in which θ is the fraction of the surface covered by thorium atoms at any time, t, in seconds and θ_r is the limiting value of deactivation for a wire of radius R in cm.

The size of grains was determined from microscopic examination of the surface with the aid of the camera lucida at a magnification of 1000. For each filament the areas of about 400 grains were measured, the distribution was plotted and

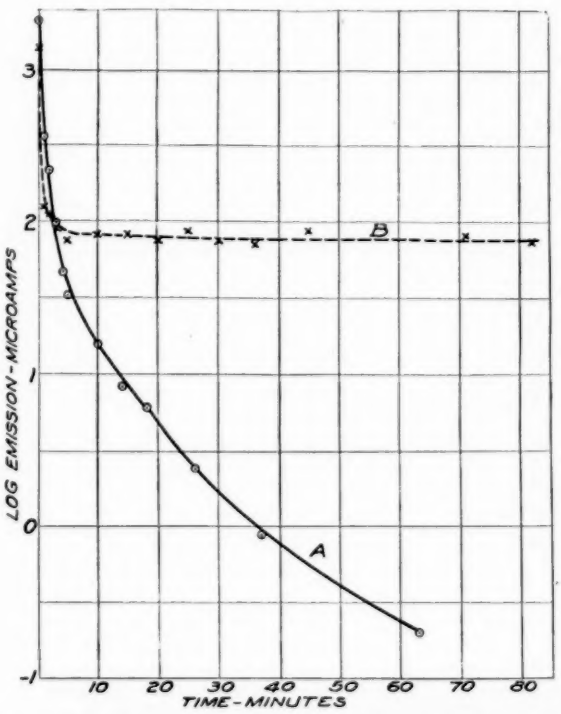

Fig. 1. Effect of grain size on deactivation of thoriated filaments at 2400°K. A is fine grained, B is long grained.

[4] Zay Jeffries, Trans. Amer. Inst. Min. Eng. **60**, 588 (1919).

the effective grain radius taken as that of the area at the point of mid-distribution.

An example is given in Fig. 1 to show the effect of grain size upon the deactivation curve at 2400°K. Both filaments are from the same wire, 0.005 cm in diameter. *A* is the untreated sample whose effective grain radius is 5.4μ, having the fine crystallization normally characteristic of thoriated wire. *B* had been given a special high temperature treatment which served to convert it into a multiple grain wire comprising about seven grains across the area of the wire, each one measuring about 3 cm long. The value of *D* was found to be 1.7 $(10)^{-9}$ cm^2 sec.$^{-1}$ for *A*, in the same range as the value reported for the same temperature by Langmuir, 3.6 $(10)^{-9}$. For *B*, *D* was reduced about one hundred-fold, to 1.1 $(10)^{-11}$.

TABLE I. *Relation between grain size of thoriated wire and diffusion coefficient of thorium through tungsten at 2400°K.*

Grain radius in μ r	Diffusion coefficient in cm^2 sec.$^{-1}$ D	r^2D	Life at 2000°K Hours
4.0	4.1 $(10)^{-9}$	65 $(10)^{-9}$	250
4.8	2.5	58	160
5.3	3.2	90	260
6.2	1.5	58	3200
6.3	2.2	87	3600
6.9	1.3	62	18000
7.3	1.3	69	5800
8.2	0.9	61	9600
8.6	1.0	74	18000
1000	0.21		2800
3000	0.01		50

More comprehensive measurements were made on a lot of thoriated wire, 0.0102 cm in diameter and containing 1.5 percent thoria. Samples were so heat treated as to cover a wide range in grain size. In the last two cases the grains filled entirely the cross section of the wire and had the average length noted. The results are given in Table I.

Table I shows a distinct trend of *D* toward lower values as the radius of the grain increases. The significance of this is that it is not the radius of the wire but the radius of the grain which should be incorporated in the formula for the diffusion. The original derivation presumed a certain concentration gradient throughout the area of the wire as a whole as expressed in the equation, $G=(2C_u/R)e^{-5.783D/R^2}$. The present results denote that it is rather the area of the grain which is the important entity and that the concentration gradient should be with reference to the distribution of thorium within each grain, with the term R^2 referring to the radius of the latter. This is brought out still more clearly in the 3d column of Table I, where a revised version of the diffusion coefficient is expressed as the product of *D*, the conventional coefficient, and r^2, the square of the effective grain radius characterizing each filament. To within the limits of error in measuring grain size, the product remains constant. Such a relationship denotes that the rate of diffusion as measured is that characteristic of diffusion within a grain and that the rate of diffusion along grain boundaries is relatively too rapid for measurement.

Saul Dushman and L. R. Koller have studied in this laboratory the deactivation of thoriated wires for differences in diameter. Their unpublished results are also in accord with the view that grain size is a predominant factor in determining the magnitude of the diffusion constant.

Additional support is given to this view by measurements on the temperature coefficient of diffusion. In Table II are given values of *D* for several different temperatures as determined for filaments of different grain size. For comparison, the Langmuir values are given in the lowest horizontal row.

TABLE II. *Diffusion coefficient of thorium through tungsten at various temperatures.*

Grain radius in μ r	Diffusion coefficient in cm^2 sec.$^{-1}$ D 2400°	2300°	2200°	2000°
5.3	3.19$(10)^{-9}$	1.48$(10)^{-9}$	5.8 $(10)^{-10}$	——
7.3	1.34$(10)^{-9}$	6.6 $(10)^{-10}$	2.18$(10)^{-10}$	——
3000	1.13$(10)^{-11}$	——	——	2.26$(10)^{-13}$
Langmuir	3.02$(10)^{-9}$	1.23$(10)^{-10}$	4.90$(10)^{-10}$	5.94$(10)^{-11}$

The logarithms of these values of *D* are plotted against the reciprocals of the temperature in Fig. 2. The curves are displaced relatively to one another because of the differences in grain size involved. The slope of all three, however, is identical and the same in fact as that found by Langmuir, corresponding to a heat of diffusion of 94,000 calories per g-atom. If both types of diffusion took place at measurable rates, then

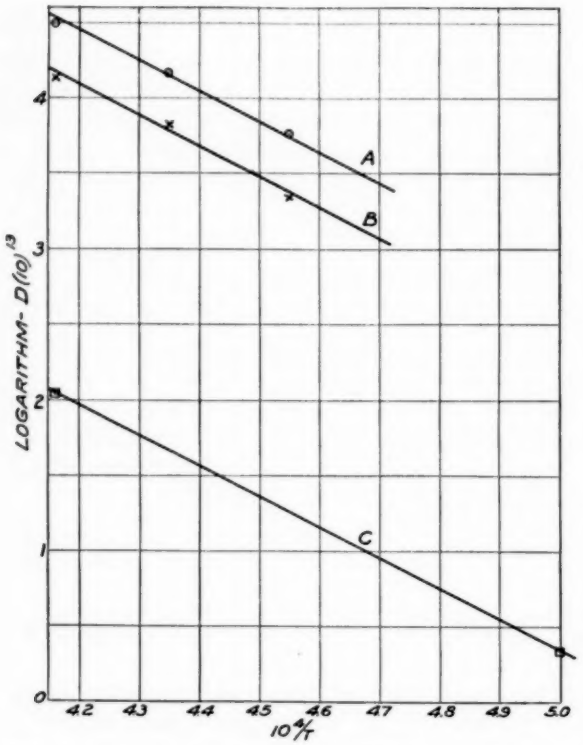

FIG. 2. Diffusion of thorium as function of temperature and grain size. *A*, 5.3μ radius. *B*, 7.3μ radius. *C*, 3000μ long.

corresponding differences in the heat of diffusion would appear in experiments covering such a wide range in grain size and one or the other type of diffusion would predominate at the extremes.

In the last column of Table I are given values for the emissive life at a temperature of 2000°K to bring out the effect of grain size upon it. The life evidently begins to become appreciable only at a grain size whose radius is about 6μ. Then it increases somewhat at least up to a grain size whose radius is 9μ. Thereafter it decreases, eventually becoming negligible for sufficiently long grains.

This is explained from the assumed relation between intergranular and intragranular diffusion and from their relation in turn to the phenomenon of induced evaporation. Whatever the mechanism of the latter may be, it seems to be unquestioned that a layer of thorium more than one atom thick is relatively unstable and that the outer layers will evaporate more readily than those atoms which are bound directly to tungsten. After the high temperature flash associated with activation, a filament has within it a certain concentration of reduced thorium. This is being continually added to, although only in small amounts, by the thorium that is reduced at the normal operating temperature. It is upon the initial concentration that dependence must be placed primarily to maintain such a gradient that the surface of the wire may be kept covered with thorium and a decrease in emission avoided. The maximum life would result when the loss by normal evaporation is just compensated for by diffusion of an equal amount of thorium from within the filament. The rate of this diffusion is given by the product DG, the diffusion constant and the concentration gradient. Only within certain critical values of D will there be an approach to the ideal compensation desired. If D is too small, which is the condition in a long grain filament, then the diffusion is obviously insufficient to maintain the full thorium coating on the surface of the wire. If the grains, on the other hand, are so fine as to give rise to too large a value of D, an equally undesirable condition exists, for the total amount of thorium diffusing is then in excess of the normal loss by evaporation and this excess evaporates from the surface of the wire so rapidly, through the phenomenon called induced evaporation, that it is virtually wasted. Such a loss lowers in turn the concentration gradient of reduced thorium which thereby falls relatively soon to such a low value that it fails to maintain an amount of diffusion that would be the equivalent of the amount normally evaporating.

ACTIVATION AND SURFACE SPREADING

The rate of activation, k, is given by the expression $d\theta/dt = k(1-\theta)$. At a temperature of 2050°K the evaporation of an adsorbed film of thorium is so extremely slow that k is proportional to the product DG (Langmuir[1]). One should expect therefore that the differences that have been found in the diffusion constant, as defined by D, should be accompanied by similar changes in k. Such differences in k have already been noted in unpublished work carried out in this laboratory by D. M. Dennison.

This relationship is manifested by the present experimental results, as is evident from the

definite trend shown in Table III. The determination of k was in each case preceded by a 3 min. flash at 2800°K to bring G to a constant value.

These results suggested a means of determining whether thorium atoms can spread over the surface of a filament. In the light of the present conception, thorium is diffusing to the surface throughout the length of the filament. The diffusion outward through a grain boundary will convey, however, many more thorium atoms to the surface at the intersection of two grains and therefore give rise to a higher concentration along the boundary than can take place on the surface of a grain as the result of direct diffusion only through the grain itself. This is by reason of the large internal volume of filament that feeds into a grain boundary. It was aimed to find if the high thorium concentration formed at grain boundaries led to a spreading of thorium over the surface of adjacent grains. The experiment was carried out by making up a filament in the form of a U, each leg being 7 cm long joined by a 1 cm length at the bottom. The legs were converted into grains about 2 cm long by flashing on separately at 3000°K in hydrogen and raising the temperature to 3300°K in the course of one minute. The 1 cm length at the bottom was rendered finely granular with an average grain radius of 4μ by raising in temperature from 1200° to 3000°K in the course of 5 min. When this filament was made into a kenotron, its rate of activation at 2050°K was found to be 5.3 $(10)^{-4}$. The emission as read at 1500°K rose to a maximum value of 1780μa as compared to a value of 5000μa customarily found for a filament of the same total length, 15 cm, but entirely fine grained. This corresponds to a value of θ for the entire filament of 0.88. The fine grain portion of the filament represented 6.7 percent of the total area and if the covering of the surface by thorium had been confined to it, the emission would have risen only to 334μa. The validity of the experiment was established by cutting off the fine grain portion of the filament and remounting the remainder in a length of 11 cm. The activation constant was thereupon found to be reduced to 1.6 $(10)^{-5}$. At the end of 5 hours, the time required to reach maximum emission when the fine grain portion was attached, its emission had risen only to 32μa. The results give a clear demonstration, therefore, of the dependence of the activation constant upon grain size and also of the occurrence of spreading of thorium atoms over the surface of tungsten.

TABLE III. *Relation between grain size and activation constant at 2050°K.*

Grain radius μ	Activation constant k
4.0	10.9 $(10)^{-4}$
4.8	17.2
5.3	10.0
6.3	8.9
6.9	4.2
7.3	5.9
8.2	4.6
8.6	3.3
3000	3.2

Gehrts[5] has derived the Langmuir equation for activation on different assumptions—namely, that activation depends primarily upon the speed with which thorium atoms spread over the surface of a crystal from grain boundaries as sources and that induced evaporation is absent. In certain special cases, as in that just described of a single crystal adjoining a mass of fine crystals, the speed of activation of the composite filament depends, of course, upon the speed of spreading and it would be possible to perform the experiment in such a way that the speed of spreading over the single crystal could be measured separately. For filaments of uniform grain character, however, the observations given above on the dependence of deactivation and life upon grain size would seem to involve diffusion as the fundamental phenomenon.

Emission of Single Crystals and Strain

Clausing[6] concluded that intragranular diffusion is altogether negligible because of his inability to develop any activation in Pintsch single-crystal filaments. We found, likewise, that Pintsch filaments could not be activated to any appreciable emission at the normal activating temperature of 2050°K or higher. In the light of the present experiments this does not mean that intragranular diffusion is negligible but that it

[5] Gehrts, Zeits. f. tech. Physik **12**, 66 (1931).
[6] Clausing, Physika **7**, 193 (1927).

can advantageously be measured at this temperature only on a multigranular wire. At 2050° the diffusion in a single crystal brings so little thorium to the surface in unit of time that the most of it is lost by normal evaporation and no opportunity given for accumulation of any perceptible amount. We were able, however, to activate the Pintsch single-crystal wire to its full emission by heating for 600 hours at 1750°K, a temperature so low that evaporation does not enter as a disturbing factor.

From tests of Pintsch filaments in incandescent lamps there was evidence that mechanical strains could be introduced that were insufficient to cause recrystallization but which were nevertheless severe enough to weaken the lattice structure. Filaments 0.004 cm in diameter were coiled on a 0.025 cm mandrel and then uncoiled, so that their final form was once more that of a straight filament. When these were tested at 2600°K in vacuum lamps, their life was found to be reduced to 20 percent for the reason that they failed by burn-out after losing only 9.6 percent in weight. Untreated filaments continued burning until they had lost 23.6 percent in weight. Similar tests on drawn wire failed to show any differences due to coiling. The Pintsch filaments which had been coiled retained their single-crystal structure so far as outward appearances showed. Microscopic examination at 1000 magnification after burning showed the uniform surface of a single crystal, free from any grain boundaries. Burning the filaments in argon developed a hexagonal cross section, which was uniform throughout their length. This is a very delicate test, as the presence of a separate grain shows up distinctly by the abrupt change in orientation of the flat crystal faces. The conclusion therefore was that the coiling had not led to recrystallization but only to the shattering of certain transverse lattice sections and that premature burn-out had occurred at one of these points.

In order to find to what extent such effects might simulate grain boundaries, a similar Pintsch filament was given the same coiling treatment and tested in a kenotron. It did in fact behave like a fine grain filament activating at the normal rate of 9.7 $(10)^{-4}$ to full, normal emission. Despite this behavior which was typical of that of a fine grain filament, microscopic examination of the surface failed here likewise to reveal any departure from a single crystal, indicating that whatever sections were serving to simulate grain boundaries in furthering the diffusion of thorium were of atomic dimensions. They can perhaps be regarded as slight displacements of the lattice, insufficient to introduce any marked change in orientation. The effect is of similar nature to certain colorations observed by Przibram[7] in single crystals of sodium chloride under radiation from β- and γ-rays from radium. When one portion of the crystal was very slightly deformed by pressure from a cube face, diagonal planes of coloration were produced throughout the underlying portion at an exposure insufficient to produce a general coloration. These planes coincided with the direction that would be expected as the result of a mechanical displacement.

After this filament had been burned for 550 hours at 2000°K, it was reactivated at 2050°K. The value of K was found to have fallen to 1.4 $(10)^{-4}$, indicating a partial healing of the hypothetical displaced section of the lattice.

In closing we wish to express our appreciation of the continued interest and encouragement shown us by Dr. Saul Dushman.

[7] Przibram, Zeits. f. Elektrochemie **38**, 490 (1932).

Experiments on the Contact Potential of Zinc Crystals

W. A. ZISMAN AND H. G. YAMINS, *Research Laboratory of Physics, Harvard University*

(Received November 7, 1932)

IT is well known that the experimental study of the Volta effect of metals in gases is difficult. Two facts have been established. Firstly, different methods of preparing the metal surfaces such as the use of various types of abrasives or cutting tools caused the contact potential difference to vary as much as 100 percent. Secondly, the potential difference varied with the time after preparation of the surface, apparently due to gas adsorption and corrosion of the metal.

Despite the above difficulties every few years experiments appear in the journals repeating the same sort of experiment and leaving everyone more firmly convinced than ever of the futility of studying the Volta effect except under high vacuum conditions. Of course, research on thoroughly degassed metals in high vacuum is necessary to obtain intrinsic contact potential differences. Yet further work on the Volta effect when adsorbed gases are present in large amounts is interesting because of its intimate connection with the study of adsorption and corrosion. In this connection the vibrating condenser method[1] used by us is ideal because of the ease of taking measurements in rapid succession after preparation of the surface.

It has never been ascertained what share of the variability with methods of cutting and polishing is due to the alterations in the structure of the surface of the metal. The cleaved surface of a single crystal is the nearest to a reproducible one that we can obtain, and hence gas should be adsorbed on such a surface in the most repeatable manner possible. Consequently, the contact potential difference between a single crystal cleaved in air and some standard metal should be reproducible.

Single crystals of pure zinc obtained from the New Jersey Zinc Company were cleaved along the basal plane, and the contact potential difference with a standard electrode was observed as it varied with time. The standard electrode was a gold plate well aged in air. Measurements of the potential differences were made with the vibrating condenser method of Zisman.[1] In our apparatus the vibrator plate was fastened to the diaphragm of a telephone receiver driven by an audiofrequency vacuum tube oscillator.

In Fig. 1 is given a typical graph of the change of the potential difference with time after cleavage of the crystal. Some ten such cleavages were made, and the time curves were found to be reproducible to 1 percent. This is a vast improvement over any other work known to us on the Volta effect of zinc in air. For instance, if the surface of polycrystalline zinc is prepared by turning in a lathe with a clean tool, the time curves obtained for successive turnings vary by 10 percent. If the surface is scraped, the variation is as much as 30 percent.

A comparison of the time curves for turned polycrystalline zinc with those for a cleaved crystal reveal that the potential differences are about 40 percent lower for the former. For example, a number of runs on polycrystalline zinc netted a mean potential difference with gold of 0.85 volts five minutes after turning, whereas the potential difference of a cleaved crystal at the same time was 1.22 volts. On the other hand, when the basal cleavage plane of a single crystal was turned in a lathe, the e.m.f.-time curves were precisely like those for the turned surface of polycrystalline zinc. This suggested that the lower values for the turned surfaces as compared with cleaved surfaces might be associated with the relatively greater roughness of the former. It is well known that roughness of surface is believed to bring condensation due to the lower vapor pressure of a liquid in a small cavity as compared with that at a flat surface. However, when the single crystal was scraped in a lathe with a razor blade, the time curves showed that the potential difference was 0.65 volts five minutes after scraping, which is even lower than for the turned surface, though the scraped surface

[1] W. Zisman, Rev. Sci. Inst. **7**, 367 (1932).

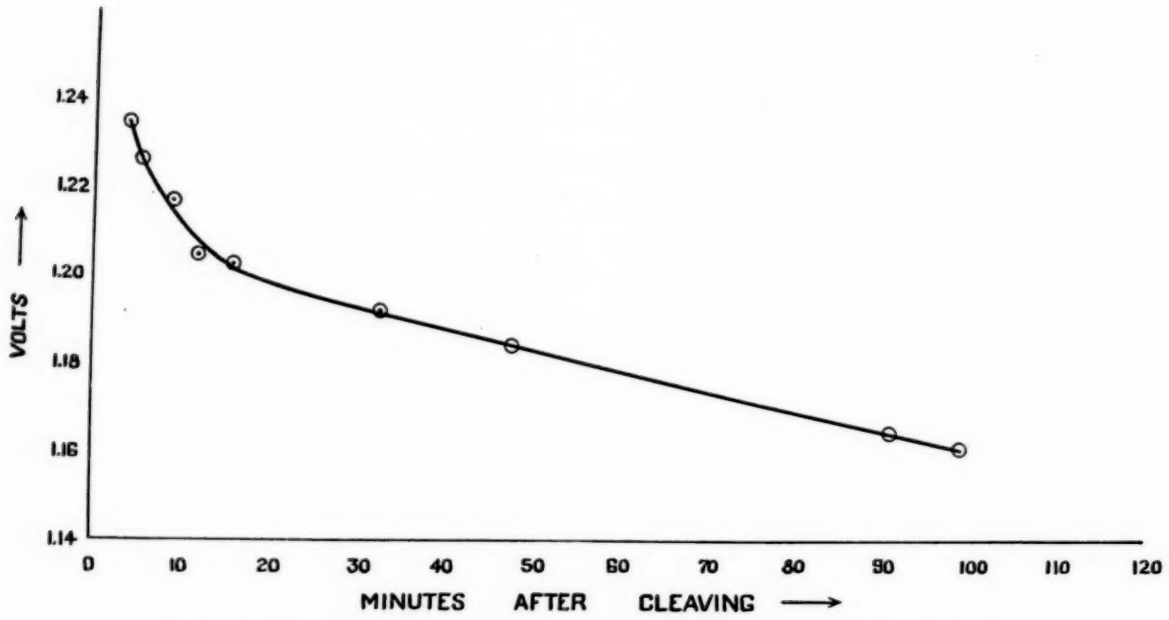

FIG. 1. Contact potential difference between a zinc crystal and a standard gold plate.

was smoother than the turned. Thus, the lower value of contact potential difference cannot be associated with greater roughness.

The turning or scraping of a metal like zinc involves a rolling and also a tearing action. It is well known[2] that rolling zinc causes about 70 percent of the small crystals in the surface to orient with their hexagonal axes making an angle with the metal surface of less than 45°, i.e., rolling causes a departure from the orientation existing in the metal before the surface was cut or scraped. Now, if the small crystals of zinc have a greater contact potential difference with gold on the basal plane than on the prism faces, then precisely the observed effects would be predicted. Turning a single crystal would cause a drop in the contact potential difference because it caused the cleavage surface to be broken into small crystals no longer oriented in the original direction with the hexagonal axes perpendicular to the surface. Scraping would make the potential difference drop even more, because it involves more of a rolling effect than does turning. The same order of magnitude of potential difference would be expected whether we turned a single crystal, a polycrystalline aggregate composed of very small crystals, or one containing very large crystals. Such was found to be the case. Successive turnings using the same type of tool and tool adjustment do not produce precisely the same distribution of orientations among the crystals each time, and hence the potential difference for turned surfaces would be expected to vary from run to run, as has been observed.

In accordance with these ideas, one would not expect any such variability with successive turnings when a metal like polycrystalline copper is used instead of zinc, for the copper crystals are each cubic, and therefore isotropic, whereas zinc is hexagonal and anisotropic. The anisotropy of zinc with respect to electrical resistivity and thermoelectric effect is well known. Thus, it is not surprising that it is also anisotropic with respect to the Volta effect.

Successive turnings of polycrystalline copper in a lathe produced e.m.f.-time curves which were identical to within ¾ percent. Furthermore, unlike zinc, the scraped copper surface behaved precisely like the turned one. These two results on copper, reproducibility with successive turnings and identity of results of turning and scraping agree very well with what would be predicted by the above idea of anisotropy of the Volta effect.

In connection with this idea of anisotropy recent experiments of Nitzsche[3] are of interest. He

[2] Wien-Harms, Handb. d. Physik **5**, 79 (1932).

[3] A. Nitzsche, Ann. d. Physik [5], **14**, 463 (1932).

found from a study of the photoelectric work function of cleaved surfaces of zinc crystals that the work function for the basal cleavage plane was 0.2 volts greater than that for the secondary cleavages planes perpendicular to the basal plane. We attempted to obtain zinc crystals that could be cleaved in these secondary planes as well as the basal plane, but so far have been unable to do so. Further experiments in this direction are planned, for it would allow us to obtain more definite evidence of an anisotropy of the Volta effect in zinc.

Some experiments on the use of abrasives like emery or of polishing agents like rouge in smoothing the surfaces of metals for the study of contact potential differences may be of interest here. Experiments dating as far back as 1880 demonstrated that the contact potential difference varied for surfaces rubbed with various types of abrasives like emery paper and sandpaper. As in the above case of a turned surface, the evident interpretations made then and continued until quite recently have been that according as one roughened the surfaces of the metal differently, so the adsorbed gas layer was altered, and hence the potential difference changed. In other words the variability obtained with abrasives was ascribed to the difference they caused in the roughness of the metal. In 1929 Ende[4] reported experiments on the Volta effect in air using two pieces of metal from the same bar such as brass or nickel. The two like metals were polished with emery or else scraped or turned in a lathe. The first treatment produced contact potential differences between the two like metals as great as 0.5 volts, whereas in the last two the resulting potential differences were always less than 0.05 volts. He suggested that emery left imbedded in the metals gave rise to a false potential difference of as much as 0.5 volts.

We found that polycrystalline zinc or a cleaved crystal when polished with emery gave rise to a potential difference with gold of about 1.30 volts. When the surface was washed with water and dried the potential difference dropped to 1.10 volts. This decrease was not due to any effects of the water, for when a polycrystalline surface free from emery was well washed with water, the potential difference after drying was within 0.01 volts of the value before washing. Thus, the polishing of turned polycrystalline zinc with emery paper raised the potential difference from 0.85 volts to 1.30 volts, because the polishing imbedded emery in the zinc. Washing with water lowered the potential difference to 1.10 volts, because some but not all of the emery was removed. In the same manner, polishing the zinc surface with rouge caused the potential difference to drop to 0.6–0.7 volts. After washing with water it rose to 0.8–0.9 volts, due to the removal of some of the rouge. These results therefore demonstrate the correctness of Ende's suggestion. A number of experiments have been published in the past decade in which emery paper was used on metals which were later introduced into high vacuum systems for measurements of contact potential differences or thermionic work functions. The above experiments show the use of emery to be an unexpected source of complications.

Conclusion

Experiments were made proving for the first time that it is possible to obtain a reproducible contact potential difference on zinc in air at ordinary pressures, provided the cleaved surface of a single crystal is used. It is suggested that the lack of reproducibility of the Volta effect of turned or scraped surfaces of zinc is due to an anisotropy in the zinc crystals with respect to the Volta effect, and not due to condensation phenomena accompanying the roughness of the surface. Confirmatory evidence is found in the reproducibility of the contact potential difference of turned and scraped surfaces of copper. Ende's suggestion that emery imbedded in the metals gives rise to false potential differences is demonstrated to be correct. It is found that emery increases the potential difference between zinc and gold by about 0.4 volts, and rouge decreases it by about 0.5 volts.

We wish to thank the New Jersey Zinc Company for furnishing us with the two single crystals of pure zinc used for these experiments, and to express our appreciation to the department of physics of Harvard University for their courtesy in allowing us to perform these experiments in the new research laboratory.

[4] W. Ende, Phys. Zeits. 30, 477 (1929).

On the Piezoelectric Properties of Tourmaline

GERALD W. FOX AND MORRIS UNDERWOOD, *Physics Laboratory, Iowa State College*

(Received October 13, 1932)

Oscillating piezoelectric plates of different frequencies have been made from California and South African Tourmaline. These plates have a frequency response of approximately 3770 kc per millimeter of thickness. The temperature coefficient for both specimens was found to be negative and is about 35.5 parts per million per degree centigrade for the African specimen and 38.1 parts per million per degree centigrade for the California crystal. Comparison of the tourmaline plates with a Y-cut quartz plate of the same size and frequency shows the tourmaline oscillators decidedly inferior on the basis of power output.

INTRODUCTION AND STATEMENT OF THE PROBLEM

SINCE Cady's[1] original discovery, the use of quartz plates to stabilize the frequency of vacuum tube oscillators has become a universal practice. Intense experimental investigation[2] has led to applications of great practical importance as well as to discoveries that yield considerable information concerning the general nature of the crystal state. According to F. Pockels,[3] twenty of the thirty-two possible crystal classes should show piezoelectric properties. However, simple exhibition of piezoelectric properties does not mean that a crystal will be useful for frequency control. This is well evidenced in the case of Rochelle salt which is highly piezoelectric but is mechanically so weak that it is entirely unsuited for use as a resonance oscillator.

In the entire list of known piezoelectric crystals, there are few of value for frequency control. Aside from quartz and tourmaline and possibly boracite, all appear worthless for one reason or another.

The present investigation of the piezoelectric properties of tourmaline proposed to determine its frequency constant and temperature coefficient, and compare it so far as possible with quartz.

DESCRIPTION OF THE CRYSTAL

Crystallographically, tourmaline belongs to the trigonal system. It is an example of class 20 (ditrigonal pyramidal) and is of the type ditrigonal polar, having one trigonal axis and three symmetry planes intersecting in it. Its chemical constitution is somewhat variable though its formula is sometimes written as ($H_6Na_2F_4B_6Al_3Si_{12}O_{63}$). A diagram of the crystal model is shown in Fig. 1. The Z axis is the polar axis as well as the optic axis. Pressure applied along this axis results in a separation of charges at the ends.

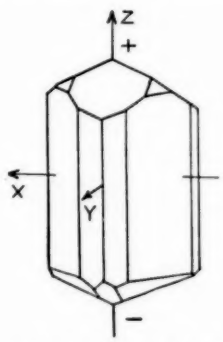

FIG. 1. Crystallographic model of tourmaline.

Tourmaline is a fairly common mineral. Gem quality crystals found in the United States come principally from Oxford County, Maine, and San Diego County, California. Most of the world's supply, however, comes from Brazil and South Africa. Crystals used as piezoelectric oscillators must be especially perfect and even those which pass for gem quality are usually not good enough. Minute flaws and cracks throughout the body of the crystal are very common and, although such imperfections are tolerated in other uses, for oscillating plates, the section must be entirely free from them. The crystals occur in a great variety of colors, often with different colors ap-

[1] W. G. Cady, Proc. Inst. Rad. Eng. **10**, 83–114 (1922).

[2] P. Vigereaux, *Quartz Oscillators and Resonators.* Excellent Bibliography, H. M. Stationary Office, London.

[3] F. Pockels, Winkelman's Handbuch der Physik, Vol. 2.

pearing in the same specimen. Tourmaline is harder and heavier than quartz, hardness being 7.5 and specific gravity about 3. On the gem market, prices for the raw crystals vary somewhat, but average around one dollar per carat for the best quality. Unfortunately, the cross-sectional areas of these crystals are small; one having a cross section of one square centimeter would be considered large.

Preparation of Plates

From a large number of specimens, two were chosen as having possibilities for use as oscillators. One of these was from California and was approximately three cm long and about eight mm in largest diameter. It shaded from pink at one end to light green at the other. Except for a six mm section near the center, this crystal was flawed for its whole length. The other, a South African specimen, was about the same size. It was deep green in color and was only slightly flawed near one end. With a lapidary's saw, fifteen sections perpendicular to the Z axis (Fig. 1) were cut from these two crystals. These pieces varied from 3 mm to 0.5 mm in thickness. Finishing the plates is a tedious process, at least when done by hand. It consists of grinding down the rough blanks by rubbing them on a plate glass slab with water and fine carborundum powder. The blanks are so small that it is difficult to hold them. The entire process is similar to the preparation of quartz plates except that it seems to require more care. In the case of quartz, it is well to have the faces parallel to within 0.01 mm, but this accuracy is not good enough for tourmaline. Likewise, the edges of the plates need to be rounded off very carefully. The most minute unevenness or chip appears enough to prevent oscillation. Because of the small cross sections, no attempt was made to cut round disks from the blanks. Their finished shape corresponded to that of the crystal cross section except that the corners were rounded off. Fig. 2 shows two of the finished oscillators. The dark one is from the African crystal; the light one, from the California specimen.

Wave-Length and Frequency Constant

The curve of Fig. 3 shows the wave-length to which the plates were resonant plotted against their thickness in mm. The points fall closely on a straight line, each point representing a separate finished plate. Both kinds of tourmaline used are represented, so that one would conclude the color

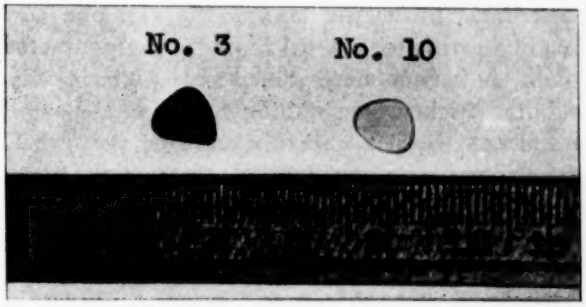

Fig. 2. Finished tourmaline oscillators. No. 3 from S. African crystal, No. 10 from California specimen.

is not an important factor. The equation of the curve is very closely: $\lambda = 79.5\ m$ where λ is the wave-length and m is in meters per millimeter. In terms of frequency: $n = 3770$ kilocycles per millimeter. Recently Straubel[4] announced the use of

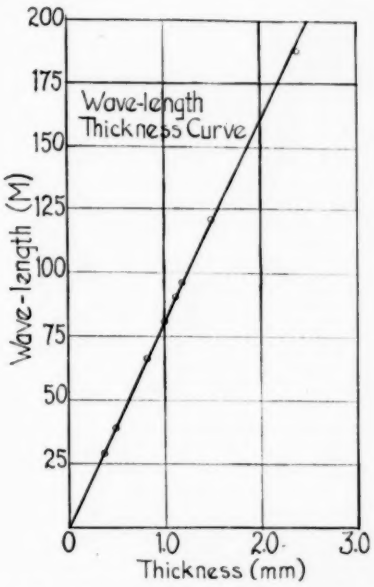

Fig. 3. Wave-length thickness curve for tourmaline. Plates from both specimens are included in the curve.

tourmaline plates for ultra high-frequency control. His plates were made for him by the firm of Carl Zeiss and from his article one would conclude that it was quite simple to make tourma-

[4] H. Straubel, Phys. Zeits. **32**, 937–941 (1931).

line plates having a fundamental wave-length of five meters, i.e., fundamental frequency of 56 megacycles and even higher. At the present time in this country, certain firms have such plates on the market and in a recent article,[5] their use was described. From the curve (Fig. 3), one can readily estimate the thickness of a five-meter plate. A twenty-meter tourmaline plate is only slightly thicker than a quartz plate of the same frequency. Both are so thin as to be very weak mechanically. A five-meter tourmaline plate would be thinner than the paper on which this is printed and, as such, would be a very delicate affair indeed. From our experiments, it seems doubtful if plates having a fundamental of this high value can be successful practically.

Temperature Coefficient

The temperature coefficient was determined for both specimens of tourmaline. Two plates cut from each crystal were carefully ground until their frequencies were within about two hundred cycles of each other. All four plates had frequencies close to 3500 kc. The conventional oscillator circuit was used in which the crystal is connected between the grid and ground, in parallel with a resistance for obtaining the proper bias. Two separate units with pentode tubes (UX 247) provided plenty of output even though the plate voltages were kept low (100 volts) to avoid unnecessary heating. Only a few minutes were required for steady conditions, and the beat note, heard on a high-frequency receiver with loud speaker, would remain constant for long periods. The room temperature was found not to vary appreciably over the one and a half hour period necessary for a run. A heavy brass plate with a light upper electrode provided the mounting for the constant temperature plate. The other mounting was similar except that the whole assembly was encased in a Pyrex tube and surrounded by a heater coil. A thermometer reading to 0.1°C was hung along side this tube for temperature determinations.

The beat frequency was measured by a siren disk driven by a smoothly variable d.c. motor with heavy duty storage battery supply. A Weston voltmeter tachometer measured the motor speed directly. This scheme proved entirely satisfactory for the precision expected and it was quite easy to determine zero beat between the siren note and the beat frequency of the crystal oscillators. Tables I and II give typical sets of data starting at room temperature and going to 50°C and back. The curves of Fig. 4 are these

[5] James Millen, Radio News **14**, 206–208 (1932).

Table I. *Frequency variation with temperature for plates 3 and 5 (African tourmaline).*

Temperature (0°C)	Siren speed r.p.m.	No. holes	Frequency (calc.)
27.5	645	54	580
29.4	410	54	369
35.2	576	54	467
38.8	1290	54	1161
41.2	995	96	1592
46.2	1275	96	2040
49.0	1560	96	2496
41.3	995	96	1592
37.1	1115	54	1004
35.0	720	54	648
27.6	450	48	350

Table II. *Frequency variation with temperature of plates 2 and 10 (California tourmaline).*

Temperature (0°C)	Siren speed r.p.m.	No. holes	Frequency (calc.)
26.4	795	96	1272
30.5	595	48	476
34.6	0	0	0
39.2	905	48	724
40.8	1425	48	1140
44.1	1075	96	1720
49.1	1225	96	2464
45.7	540	96	1960
38.6	0	96	428
33.0	615	0	0
30.1	1215	48	492
—	—	—	—

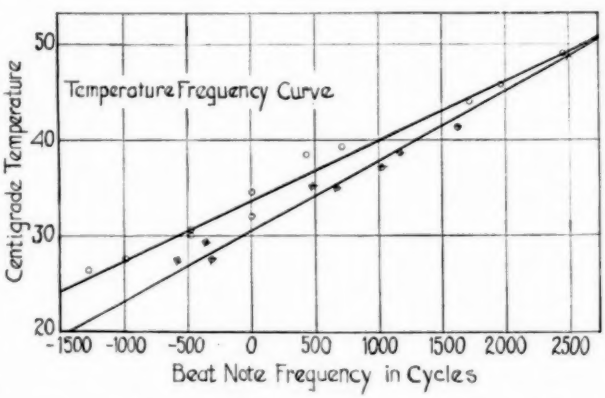

Fig. 4. Temperature frequency curves for tourmaline. The upper curve represents the African crystal, the lower one the California oscillators.

data plotted. The frequency variation is evidently linear over the range investigated and, as calculated from the upper curve (African tourmaline), the temperature coefficient is approximately 35.5 parts per million per degree and is negative. For California tourmaline (lower curve), the coefficient is also negative and, as calculated is 38.1 parts per million per degree.

Comparison of Tourmaline with Quartz

In order to compare the output of quartz and tourmaline, it was necessary to make a quartz plate of about the same dimensions as the tourmaline plates. Since in practice, the quartz disks are nearly always larger than a centimeter in diameter, this meant a disk of about half the customary size. A Y-cut disk of 7 mm diameter was made having a fundamental frequency of 3580 kc. With one of the pentode oscillator circuits mentioned previously, observations were made on the power dissipated in an auxiliary coupled circuit consisting of a high-frequency ammeter in series with a loop made of nichrome ribbon. The auxilliary circuit was coupled closely enough to the driver circuit to load it as much as possible without throwing it out of oscillation. The coupling was kept the same throughout the experiment with the quartz plate and during the experiments with the three best tourmaline plates. The observations made are plotted in Fig. 5, where relative power is plotted against the plate voltage on the pentode. Curve 1 represents the output of the pentode, quartz controlled. At the voltages shown, the tourmaline plates stopped oscillating. They would start again on lowering the voltage but always stopped on increasing it

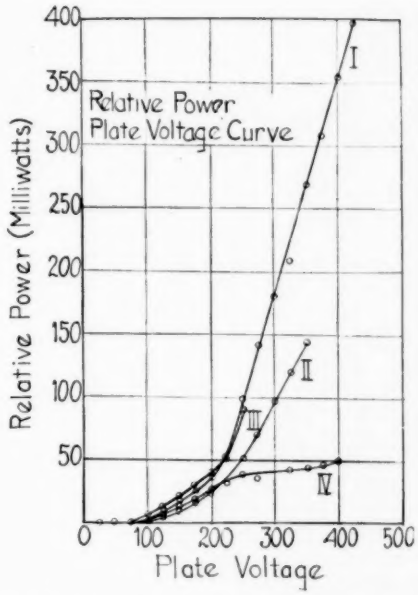

Fig. 5. Comparison of power output of quartz and tourmaline. Curve I represents the quartz. The other curves represent the three best tourmaline plates.

near the values shown. It is realized that a strict comparison would require the use of an X-cut quartz plate, i.e., one in which the applied field is perpendicular to the electric axis as is the case with the tourmaline plates. This was not available when the experiment was performed.

In general, one fails to see from these experiments, wherein tourmaline has any advantages over quartz. The cost and scarcity of the material are serious objections and the smaller size of the crystals make it more difficult to handle. For the stabilization of ultra-high frequencies, it still appears better to use quartz plates of lower frequency and triple or quadruple to obtain the short wave-length radiations desired.

The Theory of Refraction Shooting

MORRIS MUSKAT, *Gulf Research Laboratory, Pittsburgh, Pa.*

(Received October 3, 1932)

Considerations of geometrical optics indicate that the limiting rays travelling along the interface between two homogeneous elastic media should carry inappreciable amounts of energy. Nevertheless, the "first arrival" waves in refraction shooting processes, which give linear time distance curves, are usually interpreted as being due to such limiting rays travelling along the interface with the velocity of the lower medium. To clear up the situation an analysis of the problem has been made both from the points of view of geometrical optics and wave theory. It is pointed out that although the assumed "refraction" paths are minimal time paths in the sense of Fermat's principle the applicability of the latter along a surface of discontinuity may be open to question. On the other hand, it is proved that, geometrically, they are necessarily real, since they are the only type of path that can give the observed linear time distance curves. The wave theory treatment of the problem for fluid media modified slightly from the operator method analysis previously given by Jeffreys, is then presented to show that the wave theory actually gives waves whose geometrical interpretations are exactly those of the refraction shooting process. Their amplitudes vary inversely as the square of the distance from the source and they give vertical displacements of the same order as those of the directly reflected waves. The analysis is extended to the case of general elastic media and it is shown that *four* types of "refracted" waves will be produced upon the incidence at the interface of either a longitudinal or transverse wave pulse. Two of the waves will be recorded as longitudinal waves and the other two as transverse. One of each pair effectively travels in the second medium with the longitudinal velocity of the medium and the other two travel with the transverse velocity of the lower medium. The velocities and accelerations produced by these "refracted" waves will vary over the pulse thickness exactly as the displacements and velocities in the incident pulse.

IT is an established practice in applied geophysics to assume that the refraction paths of the seismic waves in a "refraction shooting" process have a form equivalent to that indicated in Fig. 1.

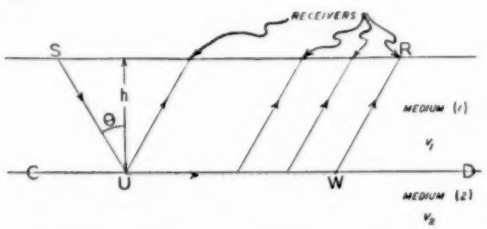

FIG. 1. Diagrammatic representation of "refraction" paths usually assumed in geophysical analyses.

The feature of these paths which gives them the role of refraction paths, and the main concern of the present discussion, is, that according to such a representation the cone of rays incident from a source S on an interface, CD, enters the second medium, travels with the velocity of the second medium along the interface, and then emerges at various points of the interface at the angle of total reflection to be finally recorded by the seismographs at the surface SR. The reason why these paths—apparently satisfying the laws of geometrical optics—need discussion, is that from an energy point of view they would be expected to carry inappreciable, if any, amounts of energy. In fact, if medium (2) is taken as strictly homogeneous no ray entering it from medium (1), even including the limiting one at total reflection, can ever again re-enter medium (1). Thus a cone of rays impinging at any point of CD is, in general, partially reflected and partially refracted and except for incidence upon other interfaces these components suffer no further changes in their paths. In the following, it is proposed to review more critically the whole situation and to show that the detailed consideration of the wave characteristics of the problem explains the apparent discrepancies.

THE MINIMAL TIME CHARACTER OF THE REFRACTION PATHS

It is well, however, first to look more closely at the practical problem which apparently requires the assumption of such paths as are drawn in Fig. 1. In this regard it is to be remembered that these paths are specifically intended to carry

the "first arrival" impulses from the sources S to the receivers at R. That is, they are the paths along which the time of transmission of the impulse is a minimum. That they satisfy this requirement is readily shown by the following elementary calculation. Denoting SR by x, and the depth of CD below SR by h, the time of travel along a path incident on CD at θ, is evidently:

$$t=x/v_2+2h\{\sec\theta/v_1-\tan\theta/v_2\}, \qquad (1)$$

where, as usual, it is assumed that $v_2>v_1$. This has a minimum,

$$t_{\min.}=x/v_2+2h\cos\theta_t/v_1 \qquad (1a)$$

at the angle of total reflection

$$\theta_t=\sin^{-1}(v_1/v_2). \qquad (1b)$$

Further, $t_{\min.}$, as given in Eq. (1a), is smaller than t_r which corresponds to the directly reflected ray and is given by:

$$t_r=(x^2+4h^2)^{1/2}/v_1 \qquad (1c)$$

since:

$$t_r^2-t^2_{\min.}=(1/v_1^2)(x\cos\theta_t-2\mathrm{h}\sin\theta_t)^2. \qquad (2)$$

In the sense that Eq. (1a) shows that the refraction paths of Fig. 1 represent minimal time paths, they satisfy the requirements of Fermat's principle. However, one may question the significance of this since the paths in which the sections UW are traversed in the first medium are certainly "neighboring paths" in the sense of Fermat's principle, and yet require times greater than $t_{\min.}$ by finite amounts. In fact, the applicability of Fermat's principle for paths parallel to surfaces of discontinuity does not seem to have been established as yet by any detailed analysis and a minimization on one side of such a surface may be open to question. But even granting the validity of the process used in deriving Eq. (1a), its correctness does not of itself imply that appreciable amounts of energy will actually travel along these geometrical paths.

The Implications of a Linear Time Distance Curve

In view of this lack of conclusiveness of these geometrical path arguments, with regard to the reality of the supposed refraction shooting paths it is of importance to see how necessary they are from an empirical point of view. And here the implications are more definite, although the totality of the significant empirical data states the single fact that in many observed cases the time of first arrival at the receivers R varies linearly with the distance between the receivers and the source, i.e.,

$$t=ax+b. \qquad (3)$$

Of course, in many cases there is a curvature to the "time distance" curves but of importance here is the fact that there are definitely some whose linearity is exact within the experimental errors. It should be mentioned, too, that relations as Eq. (3) do not hold for all values of x. For small values of x the direct wave from S to R will come in first, and only after $x>2h[(v_2+v_1)/(v_2-v_1)]^{1/2}$ will a wave governed by Eq. (1a) come in sooner.

The question then is: what, if any, are the implications of Eq. (3) with regard to the paths along which the "first arrivals" travel? To answer this question it is convenient to set up a general relation for the time required for a wave to traverse any general type of path.

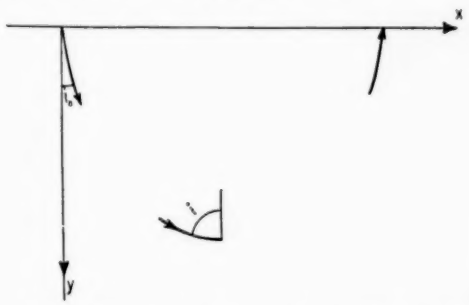

FIG. 2. Path element of a general seismic wave path.

Thus let us suppose that the wave reaching the distance x, from its shot point, at the time t has left the shot point at the angle i_0 with the vertical; and let its angle with the vertical along any element of its path be i. If the velocity (variable only with the depth) at this element is v, which we may leave perfectly arbitrary, we must have by the generalized law of refraction:

$$\sin i/v=\text{const.}=\sin i_0/v_0\equiv 1/\alpha. \qquad (4)$$

Considering the path as given by the curve $y=y(x)$, it is evident that $\sin i=(1+y'^2)^{-1/2}$ so that together with Eq. (4)

$$y'=(\alpha^2/v^2-1)^{1/2}. \qquad (4a)$$

The total time and distance for the path are therefore given by:

$$t = \int (ds/v) = \alpha \int (dy/v(\alpha^2 - v^2)^{1/2}) \qquad (5)$$

$$x = \int (v dy/(\alpha^2 - v^2)^{1/2}) \qquad (6)$$

so that

$$t = x/\alpha + (1/\alpha) \int [(\alpha^2 - v^2)^{1/2}/v] dy. \qquad (5a)$$

Since by assumption v depends only on y and moreover increases with y, the path is evidently symmetrical about the vertical through the point of greatest depth along the path; this is given by the value of y at which

$$v(y) = \alpha. \qquad (7)$$

The integral in (5a) can therefore be written as a definite integral from 0 to $y_{max.}$ as:

$$t = \frac{x}{\alpha} + \frac{2}{\alpha} \int_0^{y_{max.}} \frac{(\alpha^2 - v^2)^{1/2}}{v} dy. \qquad (5b)$$

Hence:

$$\frac{d}{dx}(t\alpha) = 1 + 2\alpha\alpha' \int_0^{y_{max.}} \frac{dy}{v(\alpha^2 - v^2)^{1/2}}$$

$$= 1 + \alpha' t = t'\alpha + \alpha' t,$$

and finally

$$dt/dx = 1/\alpha. \qquad (8)$$

Hence if t varies linearly with x as in Eq. (3), α must be the same for the paths terminating at the different values of x. This, however, is impossible if the path is to have a single point minimum, as implied by Eq. (5b), and as one would conclude from the observation that once α and hence i_0 is chosen the complete path with its lateral extent, x, is immediately determined. Eq. (8) nevertheless demands that if the time distance curve *is* linear, as in Eq. (3), *a given angle of entry i_0 must give rise to a number of paths.* Hence, since we must still maintain the requirement of symmetry of the paths about the midway plane, it must be concluded that these various paths arising from the single angle i_0 or single α are extended horizontally at the depth of their maximum penetration, just as the refraction paths of Fig. 1 are supposed to be. Or, stated more explicitly: No set of seismic paths suffering refraction due to a velocity distribution increasing (continuously or discontinuously) with depth, can give rise to linear time distance curves unless the paths have a common maximum penetration and continue horizontally, for variable distances at the maximum penetration.

Since as already mentioned, linear time distance curves are actually observed empirically, the above discussion may be considered as a proof by means of geometrical optics of the reality of the refraction paths of Fig. 1. These paths, then, do not represent simply a fortuitous assumption, but rather the necessary implication, from the point of view of geometrical optics, of the observed linear time distance curves.

It appears, then, that although it is difficult to see from the elementary consideration of geometrical optics principles, how the refraction paths can be of significance with respect to the transfer of energy, still the empirically established linear time distance curves do demand the postulation of these paths. To resolve this difficulty it is evident that one must make a close analysis of the details of the whole process from the wave point of view.

Before entering upon such a discussion, however, it may be of interest to suggest a physical interpretation of the refraction paths of Fig. 1 from a somewhat different point of view than has been heretofore considered.

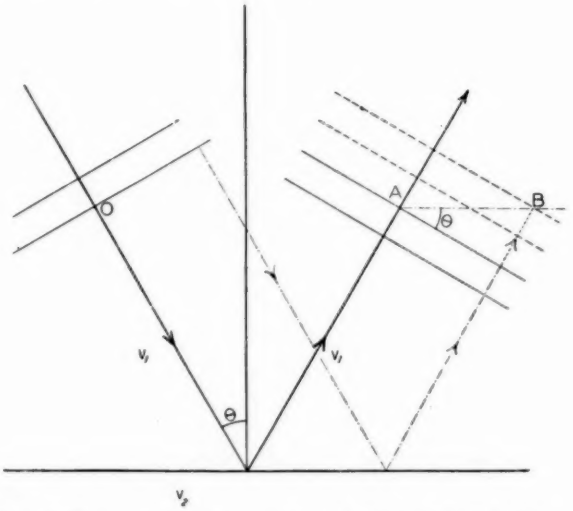

FIG. 3. Plane wave representation of the "refraction shooting" process.

Thus, as indicated in the diagram, a wave travelling with the velocity v at an angle θ with the normal has a horizontal component velocity of $v \sin \theta$, but at the same time an *apparent*

velocity as measured, for example, by the time required for an impulse, on the *same wave front*, to reach B after it has reached A, which is given by:

$$v_x = v_1/\sin\theta. \tag{9}$$

If then we consider a single plane wave pulse passing a point as O and travelling towards the interface to be reflected and observed at A and B, the effective velocity of propagation between A and B will be given by Eq. (9). Now it may be shown that the time required for a plane wave impulse passing O to reach a point as B by a direct reflection at the interface is a maximum for the regular angle of reflection, i.e., for the ray which would meet the interface midway between O and B, and is evidently a minimum for a vanishing angle. In any case, if only the times for pulses travelling at the same angle are compared, the time distance curves found at A and B will always be linear. And if bundles of pulses moving at different angles are available, those with the smaller angles should come in first. However, since the reflected amplitudes will be greater when the angles equal or exceed that of total reflection the first arrival pulse of appreciable amplitude may well be that incident at the interface at the angle of total reflection.

Since for the angle of total reflection:

$$v_x = v_1/\sin\theta_i = v_2 \tag{9a}$$

the first arrivals of appreciable amplitude would have the apparent velocity of the second medium. Further, as already mentioned, they would give a linear time distance curve.

In this way the main features of the refraction paths may be developed without any recourse to the waves actually travelling in the second medium. The refraction paths are, then really all reflection paths except that observations at successive stations are to be interpreted as relating to the *same wave front*. In this sense this point of view represents another extreme idealization. Thus whereas previously all the paths have been represented by concentrated line trajectories passing from the sending to the observing points, the above picture is based on the concept of infinitely extended plane wave fronts, different parts of which may be recorded at various stations at correspondingly different times.

Although this point of view does avoid the question of energy transfer in the ray travelling along the lower surface of the interface, it, too, is evidently greatly idealized and cannot give a complete description of the phenomena involved. In particular, the infinite plane waves are simply impossible in a finite system and certainly near the wave source the assumption is quite unjustified. On the other hand, the above point of view does serve to bring out the fact that all that we really observe at the surface are the superpositions of a number of individual wavelets in the form of a wave front, rather than a series of individually projected rays which can be separately traced back to the original source. And in fact, the wave theory analysis which we shall now present does give just this type of a representation.

Wave Theory Analysis for Longitudinal Waves

The wave theory analysis of the problem of refraction shooting has really already been given by Jeffreys[1] for the separate cases where only longitudinal or transverse waves are considered, although Jeffreys' interest in this question arose from problems of earth quake propagation. In the following, to show the method of analysis that will be used later for the more general case, Jeffreys' discussion of the problem for compressional waves will be essentially repeated although his operator method will be replaced by the somewhat more familiar differential equation analysis. Further, since we are primarily interested in the effect of the interface we shall from the outset consider the simplified problem of a single interface separating two infinite media. Jeffreys treats the case where the upper medium is bounded but then neglects the waves reflected from the upper free surface. On the other hand, we shall analyze the reflected wave in somewhat more detail than is given in Jeffreys' work, and finally, in the last section we shall treat the case of general elastic media which reveals the existence of several *types* of "refracted" waves.

In the present section, however, our problem will be to find the waves resulting from a spherical pulse emitted at a source in a homogeneous,

[1] H. Jeffreys, Camb. Phil. Soc. Proc. **23**, 472 (1926); Gerl. Beitr. z. Geophys. **30**, 336 (1931).

non-dispersive, and non-aborbing fluid medium at a height h above the interface, $z=0$. Because of the symmetry the cylindrical coordinates (ρ, z) will be used. The densities of the media will be denoted by γ_1, γ_2, and the velocities by (v_1, v_2) where $v_1<v_2$.

Since only compressional waves will be treated for the present, the problem may be described by the potential Φ where:

$$(\nabla^2+\omega^2/v^2)\Phi=0 \tag{10}$$

and the displacement components along z and ρ are given by:

$$w=\partial\Phi/\partial z; \quad q=\partial\Phi/\partial\rho. \tag{10a}$$[2]

Eq. (10) implies that the problem is in a steady state and composed of waves of the single frequency ω. The problem of the pulse will be derived by a superposition of the effects of the individual frequencies.

Fundamental solutions of Eq. (10) are of the form:

$$\left.\begin{aligned}\Phi&=e^{+\alpha z}J_0(\xi\rho),\\ \alpha^2-\xi^2+\omega^2/v^2&=0,\end{aligned}\right\} \quad \text{where} \tag{11}$$

and these must be combined so as to give a source at $(0, h)$ and also to satisfy the boundary conditions at $z=0$. To obtain the effect of the source it is more convenient, however, to simply add on directly the function

$$\Phi_0=\frac{e^{-i\omega/v}[\rho^2+(h-z)^2]^{1/2}}{[\rho^2+(h-z)^2]^{1/2}}, \tag{12}$$[3]

which satisfies Eq. (10) and represents a unit source at $(0, h)$, emitting compressional waves of frequency ω and velocity v. But since for the remainder of the solution, functions of the form of Eq. (11) will be used. Eq. (12) will also be expressed in this way. Thus from well-known results of the theory of Bessel functions we may write: for $z<h$

$$\Phi_0=\int_0^\infty \frac{e^{-\alpha(h-z)}J_0(\xi\rho)\xi d\xi}{\alpha}, \tag{12a}$$

where α is again given by Eq. (11), with $v=v_1$.

The complete solution to the problem may now be expressed as:

$$\left.\begin{aligned} z>0 \quad \Phi_1&=\Phi_0+\int_0^\infty A(\xi)e^{-\alpha z}J_0(\xi\rho)d\xi,\\ z<0 \quad \Phi_2&=\int_0^\infty B(\xi)e^{\bar\alpha z}J_0(\xi\rho)d\xi,\end{aligned}\right\} \tag{13}$$

where $\bar\alpha^2=\xi^2-\omega^2/v_2^2$, and A and B are arbitrary functions to be chosen in such a way that the normal displacements and pressures are continuous at the interface $z=0$, i.e., such that:

$$\left.\begin{aligned} w_1=\partial\Phi_1/\partial z&=w_2=\partial\Phi_2/\partial z\\ \gamma_1\Phi_1&=\gamma_2\Phi_2\end{aligned}\right\} \text{ at } z=0. \tag{13a}$$

If Eqs. (13a) should hold, A and B must be given by:

$$B=2\xi e^{-\alpha h}/(\alpha k+\bar\alpha);$$
$$A=(\xi e^{-\alpha h}/\alpha)(\alpha k-\bar\alpha)/(\alpha k+\bar\alpha); \quad k=\gamma_2/\gamma_1.$$

Hence we have finally:

$$\left.\begin{aligned}\Phi_1&=\Phi_0+\int_0^\infty \frac{\xi}{\alpha}\frac{\alpha k-\bar\alpha}{\alpha k+\bar\alpha}e^{-\alpha(h+z)}J_0(\xi\rho)d\xi,\\ \Phi_2&=2\int_0^\infty \frac{\xi e^{\bar\alpha z-\alpha h}}{\alpha k+\bar\alpha}J_0(\xi\rho)d\xi.\end{aligned}\right\} \tag{14}*$$

To interpret Eqs. (14) we shall again follow the

[2] Φ has the additional physical significance that for a harmonic wave it is proportional to the dilatation of the medium. For a general wave form the dilatation is proportional to $\partial^2\Phi/\partial t^2$. Further, its time derivative is a velocity potential and is the function Jeffreys uses.

[3] For $\omega<0$, all the succeeding formulae are to be changed to their complex conjugate values.

* It may be of interest to observe that although equations exactly equivalent to Eq. (14) occur and have been discussed in detail in the problem of the transmission of radio waves over the earth's surface (cf. Riemann-Weber, *Die Differential und Integralgleichungen der Mechanik und Physik* II, p. 541) the fact that these analyses have not led to "refraction paths" such as we shall find below, is in no way contradictory to the analysis to be given here. For in the problem of radio-wave transmission the complex velocity in the earth is in absolute value *less* than the velocity in the incident medium, air. Hence, one would not expect, even geometrically, total reflection phenomena and the associated refraction paths which arise in the seismic problem. And in fact the approximations made in evaluating the integrals of Eq. (14) for the radio-wave problem are explicitly based upon the assumption that the effective velocity contrast is just the reverse of what it is in the seismic case. In this way, together with the assumption of a complex effective earth velocity, our refraction paths are not only automatically eliminated, but at the same time the Sommerfeld surface waves are introduced as the predominant feature of the phenomena.

method of Jeffreys and of Sommerfeld.[4] Thus, first, it is convenient to separate out the second term of Φ_1 since it alone represents the reflected wave or the effect of the second medium. At the same time the change of variable: $\xi=(\omega/v_1)\eta$; $\alpha=(\omega/v_1)(\eta^2-1)^{1/2}$; $\bar{\alpha}=(\omega/v_1)(\eta^2-v_1^2/v_2^2)^{1/2}$ may be introduced. We have then:

$$\Phi_r=\frac{\omega^2}{v_1^2}\int_0^\infty \frac{\eta}{\alpha}\frac{\alpha k-\bar{\alpha}}{\alpha k+\bar{\alpha}}e^{-\alpha(h+z)}J_0\left(\frac{\omega\rho}{v_1}\eta\right)d\eta. \quad (15)$$

Evidently the integrand has branch points at $\alpha=0$, $\bar{\alpha}=0$. To define the behavior of the integrand as these points are crossed we shall take α and $\bar{\alpha}$ as positive when $\eta>1$ and make a cut in the η plane so that η moves around $\eta=1$ and $\eta=v_1/v_2$ on the positive imaginary side. Eq. (15) may now be broken up into 2 integrals by the substitution of the relation:

$$2J_0=H_0^{(1)}+H_0^{(2)},$$

where $H_0^{(1)}$ and $H_0^{(2)}$ are Hankel integrals, the former vanishing on an infinite semicircle in the upper half of the complex plane and the latter when the semicircle is in the lower half of the complex plane. Since the integrand is regular in the upper right quadrant of the complex plane and its branch points lie below the cut along the real axis, Eq. (15) may be replaced by:

$$\Phi_r=-\frac{\omega^2}{2v_1^2}\int_{t\infty}^0 \frac{\eta}{\alpha}\frac{\alpha k-\bar{\alpha}}{\alpha k+\bar{\alpha}}e^{-\alpha(h+z)}H_0^{(1)}\left(\frac{\omega\rho\eta}{v_1}\right)d\eta$$
$$-\frac{\omega^2}{2v_1^2}\int_{-t\infty}^0 \frac{\eta}{\alpha}\frac{\alpha k-\bar{\alpha}}{\alpha k+\bar{\alpha}}e^{-\alpha(h+z)}H_0^{(2)}\left(\frac{\omega\rho\eta}{v_1}\right)d\eta$$
$$-\frac{\omega^2}{2v_1^2}\oint \frac{\eta}{\alpha}\frac{\alpha k-\bar{\alpha}}{\alpha k+\bar{\alpha}}e^{-\alpha(h+z)}H_0^{(2)}\left(\frac{\omega\rho\eta}{v_1}\right)d\eta,$$

where the circuits in the last integral are infinite loops about the branch points, and which close at the infinite quarter circle.

Since $H_0^{(1)}(iz)=-H_0^{(2)}(-iz)$, the first two integrals above cancel and we are left with

$$\Phi_r=-\frac{\omega^2}{2v_1^2}\oint \frac{\eta}{\alpha}\frac{\alpha k-\bar{\alpha}}{\alpha k+\bar{\alpha}}e^{-\alpha(h+z)}H_0^{(2)}\left(\frac{\omega\rho\eta}{v_1}\right)d\eta. \quad (16)$$

Considering now the loop around the branch point at $\alpha=0$, the contribution of the small contour about the branch point itself vanishes as the loop is shrunk and one has simply the effect of α changing sign as the branch point is encircled. Thus we may set

$$\eta=1-i\theta : \theta>0. \quad (17)$$

Now since $H_0^{(2)}(z)$ vanishes exponentially for large negative imaginary parts of its argument, the integrand is small except when θ is small. We can therefore set:

$$\alpha\leqq(\omega/v_1)e^{-\pi i/4}(2\theta)^{1/2};\ \bar{\alpha}\leqq(\omega/v_1)\beta;[5]$$
$$\beta=(1-v_1^2/v_2^2)^{1/2}. \quad (17a)$$

As the branch point, $\alpha=0$, is circled and the contour returns to the infinite quadrant the sign of α is changed. Expanding the term $(\alpha k-\bar{\alpha})/(\alpha k+\alpha)$ in powers of $\alpha/\bar{\alpha}$ we have to second order terms:

$$\Phi_{r_1}\leqq\frac{i\omega^2}{v_1^2}\int_0^\infty \frac{\eta}{\alpha}H_0^{(2)}\left(\frac{\omega\rho}{v_1}(1-i\theta)\right)$$
$$\left\{\cosh\alpha(h+z)+\frac{2\alpha}{\bar{\alpha}}k\sinh\alpha(h+z)\right\}d\theta.$$

Replacing now, for ρ large, $H_0^{(2)}$ by the first term of its asymptotic expansion, and setting: $\theta^{1/2}=y$; $m=\alpha(h+z)/\theta^{1/2}$, we may rewrite Φ_{r_1} as:

$$\left.\begin{aligned}\Phi_{r_1}&=-2\left(\frac{\omega}{\pi v_1\rho}\right)^{1/2}e^{-i\omega\rho/v_1}\int_0^\infty e^{-\omega\rho y^2/v_1}\\&\times\{\cosh my+[2km/\bar{\alpha}(h+z)]y\sinh my\}dy\\&=-\frac{1}{\rho}e^{-i\omega\rho/v_1+m^2v_1/4\omega\rho}\left(1+\frac{m^2kv_1}{\bar{\alpha}\omega\rho(h+z)}\right)\\&=-\frac{1}{\rho}e^{-i\omega\rho/v_1-i\omega(h+z)^2/2\rho v_1},\end{aligned}\right\}(18)$$

where the term in $1/\rho^2$ has been dropped since an equivalent approximation has already been made in the substitution for $H_0^{(2)}$.

[4] A. Sommerfeld, Ann. d. Physik **28**, 665 (1909).

[5] It is to be noted that this approximation and the corresponding one for α in Eq. (19) really imply that β^2 is much larger than the important values of θ and this means, physically, that there is a large velocity contrast between the two media. The general features of the problem, however, will not be changed by this implied assumption. It may also be mentioned that Eqs. (17) (17a) imply that the loops are to be drawn parallel to the imaginary axis.

In a similar manner the contribution Φ_{r_2} due to the branch point at $\bar{\alpha}=0$ may be found. Thus setting:

$$\left.\begin{aligned} \eta &= \frac{v_1}{v_2} - i\theta; \quad \alpha \leqq \frac{i\omega}{v_1}\beta; \\ \bar{\alpha} &\leqq \frac{\omega}{v_1}\left(2\frac{v_1}{v_2}\theta\right)^{1/2} e^{-\pi i/4} \end{aligned}\right\} \tag{19}$$

α has the same value on the two sides of the loop while $\bar{\alpha}$ changes sign. The final result is:

$$\Phi_{r_2} = -(2iv_1^2/kv_2\omega\beta^2\rho^2)e^{-i\omega(\rho/v_2+\beta(h+z)/v_1)}. \tag{20}$$

The Reflection of Pulses

The physical meaning of the two terms Φ_{r_1} and Φ_{r_2} may be seen more clearly by forming pulses of these harmonic waves to correspond to an initial pulse formed from Φ_0. Thus we may define the incident pulse by the Fourier integral:

$$\Phi_0 = \frac{1}{2\pi(\rho^2+(z-h)^2)^{1/2}} \int_{-\infty-ic}^{\infty-ic} d\omega \int_0^{a/v_1} f(\mu) e^{+i\omega[\mu+t-(\rho^2+(h-z)^2)^{1/2}/v_1]} d\mu, \tag{21}$$

which represents a pulse defined by

$$\Phi_0 = \frac{1}{(\rho^2+(h-z)^2)^{1/2}} f\left[-t+\frac{(\rho^2+(h-z)^2)^{1/2}}{v_1}\right] : 0 \leqq -t+\frac{(\rho^2+(h-z)^2)^{1/2}}{v_1} \leqq \frac{a}{v_1} \tag{21a}$$
$$= 0 : \text{otherwise.}$$

The addition of $-ic$ to the limits of the integral in Eq. (21) has been made to take care of convergence requirements in the integrals for Φ_r that follow.

Performing now the same operation on Φ_{r_1} and Φ_r as carried out on Φ_0, we obtain

$$\Phi_{r_1} = \frac{-1}{2\pi\rho} \int_{-\infty-ic}^{+\infty-ic} d\omega \int_0^{a/v_1} f(\mu) e^{i\omega(\mu+t-\rho/v_1-(h+z)^2/2\rho v_1)} d\mu, \tag{22}$$

$$\Phi_{r_2} = \frac{-iv_1^2}{\pi k v_2 \beta^2 \rho^2} \int_{-\infty-ic}^{+\infty-ic} \frac{d\omega}{\omega} \int_0^{a/v_1} f(\mu) e^{i\omega(\mu+t-\rho/v_2-\beta(h+z)/v_1)} d\mu. \tag{23}$$

By comparing Φ_{r_1} with Φ_0 it follows that: $\Phi_{r_1} = -(1/\rho)f[-t+\rho/v_1+(h+z)^2/2\rho v_1]$

Recalling the fact that in deriving Eq. (18) we assumed that ρ is large it is evident that $\rho+(h+z)^2/2\rho$ is really an approximation to $(\rho^2+(h+z)^2)^{1/2}$. To this approximation therefore, Φ_{r_1} may be finally rewritten as:

$$\Phi_{r_1} = -(1/\rho)f[-t+(\rho^2+(h+z)^2)^{1/2}/v_1]$$
$$: 0 \leqq -t+(\rho^2+(h+z)^2)^{1/2}/v_1 \leqq a/v_1$$
$$= 0: \text{otherwise.} \tag{24}$$[6]

By comparing the argument of f with Eq. (1c) it becomes clear that Φ_{r_1} represents the wave directly reflected from the interface according to the laws of geometrical optics. Thus Φ_{r_1} is zero until the time that would be required for a ray to pass from the front of the pulse (at $t=0$) along the ordinary reflection path to the point (ρ, z). Furthermore, this reflected wave is a pulse of exactly the same form as the incident pulse. Hence Φ_{r_1} behaves as if it were emitted by the negative image of the real source in the interface, so that to the approximation that $\rho \sim (\rho^2+(h+z)^2)^{1/2}$ the radial displacements and velocities of Φ_0 and Φ_{r_1} are equal and opposite.

The vertical displacements and velocities of this reflected wave are, however, greater than for the direct wave Φ_0. This will be clear from the following list of the various displacement components in which coefficients as $1/(\rho^2+(h\pm z)^2)^{1/2}$ have been replaced by $1/\rho$ and only the terms in lowest power of $1/\rho$ have been retained:

$$\left.\begin{aligned} w_{r_1} &= -\frac{(h+z)}{v_1\rho^2} f'\left(-t+\frac{(\rho^2+(h+z)^2)^{1/2}}{v_1}\right), \\ q_{r_1} &= -\frac{1}{v_1\rho} \quad f'\left(-t+\frac{(\rho^2+(h+z)^2)^{1/2}}{v_1}\right), \end{aligned}\right\} \tag{25}$$

[6] Φ_{r_1} as given by Eq. (24) corresponds to the amplitude of a wave *totally* reflected from an interface. This is evidently due to the implicit assumption, already mentioned above, that the velocity contrast across the interface is high.

whereas:

$$\left.\begin{aligned} w_0 &= -\frac{(h-z)}{v_1\rho^2} f'\left(-t+\frac{(\rho^2+(h-z)^2)^{1/2}}{v_1}\right), \\ q_0 &= \frac{1}{v_1\rho} \quad f'\left(-t+\frac{(\rho^2+(h-z)^2)^{1/2}}{v_1}\right). \end{aligned}\right\} \quad (26)$$

It may be finally noted from these that the radial components decrease only as $1/\rho$ whereas the vertical components decrease as $1/\rho^2$. And this is to be expected since for large values of ρ the reflected wave must approach in form a longitudinal cylindrical pulse in which the radial components naturally predominate.

Returning now to Φ_{r_2}, we see clearly that since it has the term $1/\omega$ as a factor in the amplitudes for the individual harmonic waves, it must represent a wave distorted with respect to the initial pulse. Its pulse character, however, becomes immediately evident when the line contour of Eq. (23) is completed by an infinite semicircle in the lower half plane. For then, by Cauchy's theorem, it follows at once that:

$$\Phi_{r_2}=0 \quad \text{if} \quad a/v_1+t-\rho/v_2-\beta(h+z)/v_1<0 \quad (27)$$

or if

$$t<\rho/v_2+\beta(h+z)/v_1-a/v_1. \quad (27a)$$

Recalling now Eqs. (1a) and (17a), and noting the fact that a/v_1 is simply the time required for the wave pulse to travel a distance equal to its thickness it is clear that Φ_{r_2} vanishes until a time required for the pulse to traverse the refraction path of Fig. 1. In other words, Φ_{r_2} *represents a wave that has apparently travelled along the refraction path of Fig. 1.* The reality of these paths may therefore be considered as conclusively established.

Although this has been the essential aim of the above analysis it is of interest to note some of the features of this refracted wave. Thus as already suggested Φ_{r_2} itself is distorted with respect to Φ_0. However the velocity potential and displacements possess the same shape as Φ_0. Thus:

$$\left.\begin{aligned} \frac{\partial\Phi_{r_2}}{\partial t} &= \frac{2v_1^2}{kv_2\beta^2\rho^2} f\left(-t+\frac{\rho}{v_2}+\frac{\beta(h+z)}{v_1}\right), \\ w_{r_2} &= \frac{-2v_1}{kv_2\beta\rho^2} f\left(-t+\frac{\rho}{v_2}+\frac{\beta(h+z)}{v_1}\right), \\ q_{r_2} &= \frac{-2v_1^2}{kv_2^2\beta^2\rho^2} f\left(-t+\frac{\rho}{v_2}+\frac{\beta(h+z)}{v_1}\right), \end{aligned}\right\} \quad (28)$$

all with the restriction

$$0<\rho/v_2+\beta(h+z)/v_1-t-a/v_1.$$

Comparing these with the corresponding values for Φ_0 in Eqs. (21a) and (26) it will be seen that if Φ_0 has a sharp front so will the displacements of the refracted waves. On the other hand, if the displacements in the incident pulse rise sharply as the pulse is entered, the *velocity* components of the "refracted" pulse will rise sharply.

As to order of magnitude, Eqs. (28) show that both the radial and vertical components of displacement and velocity fall off as $1/\rho^2$. Hence, whereas in the incident or directly reflected pulse the radial components bear an increasing ratio to the vertical components as ρ increases, in the refracted wave they bear a constant ratio. Thus:

$$\left.\begin{aligned} &\text{while} \quad q_{r_1}/w_{r_1}=\rho/(h+z), \\ &\qquad\quad q_{r_2}/w_{r_2}=v_1/v_2\beta=\tan\theta_t, \end{aligned}\right\} \quad (29)$$

where θ_t is the angle of total reflection. q_{r_2} and w_{r_2} are therefore actually of the same order of magnitude. Incidentally, this last relation shows explicitly that the *refracted waves travel in the first medium at the angle of total reflection* just as is shown in Fig. 1.

The relative magnitudes of the refracted and directly reflected waves are indicated by the ratios:

$$\frac{q_{r_2}}{q_{r_1}}=\frac{2v_1^3}{kv_2^2\beta^2\rho}\,\frac{f[-t+\rho/v_2+\beta(h+z)/v_1]}{f'[-t+(\rho^2+(h+z)^2)^{1/2}/v_1]}, \quad (30)$$

$$\frac{w_{r_2}}{w_{r_1}}=\frac{2v_1^2}{kv_2\beta(h+z)}\,\frac{f[-t+\rho/v_2+\beta(h+z)/v_1]}{f'[-t+(\rho^2+(h+z)^2)^{1/2}/v_1]}. \quad (31)$$

It follows that the reflected wave will give the major radial effect at large distances, but that both types of waves contribute appreciably to the vertical components. In fact, taking the function f and f' to be of the same order of magnitude, $k=\gamma_2/\gamma_1\sim 1$, $v_1/v_2\sim 1/2$, and $z=h$ it follows that $w_{r_2}/w_{r_1}\sim 0.58v_1/h$. Hence, in this case, unless the source of the incident wave is distant from the interface by more than half of the wave velocity in the upper medium, the vertical displacements due to the refracted wave will even exceed those of the directly reflected wave. Of course, it will be understood that these comparisons between the various waves do not

refer to the same instant since at the very beginning of this discussion it was pointed out that for large distances the refracted wave would arrive at a given point sooner than the reflected wave. Rather, they refer to the effects of the waves at the same points at whatever times the individual waves may arrive there.

It may be concluded, therefore, that the wave theory not only confirms in every detail the reality of the paths of Fig. 1 but it shows further that the refracted waves travelling along these paths have vertical displacements of the same order of magnitude as those of the directly reflected waves, and hence will have a vertical energy flux of the same order as that of the directly reflected waves.

The following remarks, however, may be added. First, the analysis presented here has treated the case where the initial wave source is embedded in an infinite medium whereas the actual problem involves a free surface—the earth's surface. It is true that the detailed results would be modified but the essential features and existence of the refracted wave would evidently remain unaltered. In fact, the free surface can be readily taken care of, as Jeffreys has done, by adding to the real wave source its negative image in the free surface. The main new feature introduced in this way is the set of pulses reflected from this free surface but which have no bearing on the problem of "refraction shooting."

Another point that may be mentioned is that the approximation made in the above analysis that ρ has to be large really refers to the requirement that $\omega\rho/v_1$ or $2\pi\rho/\lambda$, is of the order of 1 or greater, where λ is the wave-length in the upper medium. Since ρ is always large when the whole phenomenon refers to earthquake disturbances the approximation will always be valid there. But in geophysical work where ρ/v_1 may be as small as 1/2, the approximation may seem questionable. However, in practical cases the predominant frequencies are usually of the order of 50 cycles per second or greater and then the product $\omega\rho/v_1$ will again be large and the approximation will again be justified.

General Elastic Media

Somewhat more serious, however, than these limitations of the above analysis is the fact that it has referred to fluid media, in which the transverse waves are automatically eliminated. Again the reason for this simplification has been the fact that the integrals in the general case that correspond to Eq. (14) are more difficult to evaluate completely. But since the analysis that can be carried through brings out some features that might not be anticipated, it will be briefly outlined, although in one respect the solution will still be incomplete.

For the general case where both longitudinal and transverse waves are excited at the interface one must add to the previous function Φ, another function χ, to take care of the transverse wave components.

The radial and vertical displacements for a harmonic wave system of frequency, ω, are then given by:

$$\left.\begin{aligned} q&=\frac{\partial\Phi}{\partial\rho}+\frac{\partial^2\chi}{\partial\rho\partial z}; \quad w=\frac{\partial\Phi}{\partial z}+\frac{\partial^2\chi}{\partial z^2}+\frac{\omega^2}{\bar{v}^2}\chi, \\ \left(\nabla^2+\frac{\omega^2}{v^2}\right)\Phi&=0; \quad \left(\nabla^2+\frac{\omega^2}{\bar{v}^2}\right)\chi=0, \end{aligned}\right\} \tag{32}$$

where v and $\bar{v}$ are the longitudinal and transverse wave velocities respectively and a common factor $e^{i\omega t}$ has been dropped throughout. Denoting by subscripts 1, 2, the media 1, 2 (separated by the plane $z=0$, cf. Fig. 4) the wave system resulting from a longitudinal wave source at $(0, h)$ in medium 1, may be represented as:

$$\left.\begin{aligned} \Phi_1&=\frac{e^{-i\omega/v_1(\rho^2+(h-z)^2)^{1/2}}}{(\rho^2+(h-z)^2)^{1/2}}+\int_0^\infty A_1(\xi)e^{-\alpha_1 z}J_0(\xi\rho)d\xi, \\ \chi_1&=\int_0^\infty B_1 e^{-\beta_1 z}J_0(\xi\rho)d\xi, \\ \Phi_2&=\int_0^\infty A_2 e^{\alpha_2 z}J_0(\xi\rho)d\xi, \\ \chi_2&=\int_0^\infty B_2 e^{\beta_2 z}J_0(\xi\rho)d\xi, \end{aligned}\right\} \tag{33}$$

$$\alpha^2=\xi^2-\omega^2/v^2, \quad \beta^2=\xi^2-\omega^2/\bar{v}^2. \tag{33a}$$

It will be supposed that $\bar{v}_1<v_1<\bar{v}_2<v_2$.

Expressing the first term in Φ_1 as in Eq. (12a) and applying the boundary conditions of the continuity of the displacements and stresses at the interface, the following equations are obtained:

$$\left.\begin{aligned} -A_1 \quad +\beta_1 B_1 \quad +A_2 \quad +\beta_2 B_2 \quad &= (\xi/\alpha_1)e^{-\alpha_1 h}, \\ -\alpha_1 A_1+\xi^2 B_1 \quad -\alpha_2 A_2 \quad -\xi^2 B_2 \quad &= -\xi e^{-\alpha_1 h}, \\ 2\alpha_1 A_1-\epsilon_1 B_1 \quad +2\delta\alpha_2 A_2+\delta\epsilon_2 B_2 \quad &= 2\xi e^{-\alpha_1 h}, \\ -\epsilon_1 A_1+2\beta_1\xi^2 B_1+\delta\epsilon_2 A_2 \quad +2\delta\beta_2\xi^2 B_2 &= (\epsilon_1\xi/\alpha_1)e^{-\alpha_1 h}, \end{aligned}\right\} \tag{34}$$

where $\delta=\mu_2/\mu_1$; $\epsilon=2\xi^2-\omega^2/\bar{v}^2\equiv 2\xi^2-k^2$, μ_2, μ_1 being the rigidity moduli of the media.

The determinantal denominator of the solutions for A_1, B_1, A_2, B_2 is:

$$\left.\begin{aligned} \Delta= -\alpha_1\beta_1\{k_1^2-(\delta\epsilon_2-\epsilon_1)\}^2-\alpha_2\beta_2\{k_1^2+2\xi^2(\delta-1)\}^2+k_1^2(\alpha_2\beta_1+\beta_2\alpha_1) \\ \times\{\delta\epsilon_2-\epsilon_1-2\xi^2(\delta-1)-k_1^2\}+4\alpha_1\alpha_2\beta_1\beta_2\xi^2(\delta-1)^2+\xi^2(\delta\epsilon_2-\epsilon_1)^2 \end{aligned}\right\} \tag{34a}$$

and

$$\left.\begin{aligned} \Delta A_1\alpha_1 e^{\alpha_1 h}/\xi= -\alpha_1\beta_1\{k_1^2-(\delta\epsilon_2-\epsilon_1)\}^2+\alpha_2\beta_2\{k_1^2+2\xi^2(\delta-1)\}^2+k_1^2(\beta_2\alpha_1-\alpha_2\beta_1) \\ \times\{\delta\epsilon_2-\epsilon_1-2\xi^2(\delta-1)-k_1^2\}+4\alpha_1\beta_1\alpha_2\beta_2\xi^2(\delta-1)^2-\xi^2(\delta\epsilon_2-\epsilon_1)^2 \end{aligned}\right\} \tag{34b}$$

$$\Delta B_1\alpha_1 e^{\alpha_1 h}/\xi=2\alpha_1\{2\alpha_2\beta_2(\delta-1)(2\delta\xi^2-\epsilon_1)-(\delta\epsilon_2-\epsilon_1)(\delta\epsilon_2-2\xi^2)\} \tag{34c}$$

with similar expressions for A_2, B_2.

As the above equations make it possible to write out explicit expressions for Φ_1, Φ_2, χ_1, χ_2 the problem is now formally solved. A useful discussion, however, requires the evaluation of the integrals. To carry out this evaluation one may still use the method of contour integration used in the simpler case of pure compressional waves. Thus it is quite clear from Eq. (34a) that the integrands of the integrals in Eq. (33) will have branch points in the complex plane at:

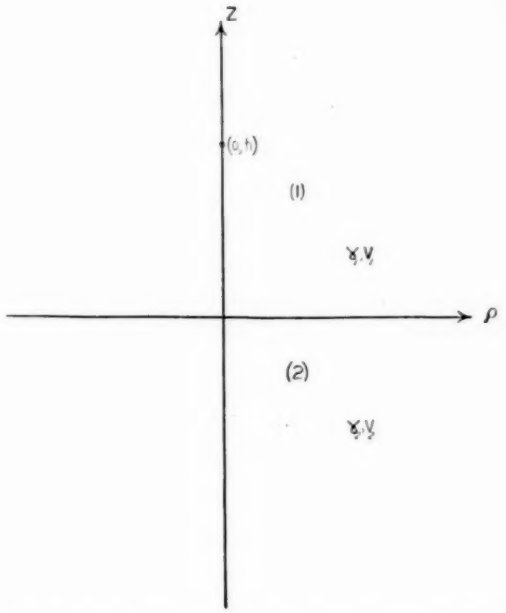

FIG. 4. Coordinate system for wave theory analysis.

$$\alpha_1=0;\quad \beta_1=0;\quad \alpha_2=0;\quad \beta_2=0, \tag{34d}$$

although the complexity of Δ makes it difficult to be certain as to whether or not there are any poles for positive values of the real part of ξ. In this respect, the present analysis will be incomplete. Nevertheless the contributions of the branch points and the general nature of the contributions of the poles, if there are any, can be readily derived.

Thus it easily follows as before that the integral in Φ_1 can be reduced to

$$\Phi_r= -(\omega/2v_1)\int A_1(\eta) \times e^{-\alpha_1 z}H_0^{(2)}(\omega\rho\eta/v_1)d\eta+T_1, \tag{35}$$

where the substitution $\xi=\omega\eta/v_1$ has been made in Eq. (35), so that $\alpha_1=\omega/v_1(\eta^2-1)^{1/2}$. The circuit for the integral is composed of loops which come from the lower right infinite quarter circle, encircle the branch points and return to the quarter circle. T_1 represents the contributions due to the poles.

Now when the loop encloses a particular branch point $\eta_0=v_1/v_0$, $A_1(\eta)$ may be written as:

$$A_1(\eta)=\frac{\eta(E+F\alpha_0)e^{-\alpha_1 h}}{(\eta^2-1)^{1/2}(E'+F'\alpha_0)}, \tag{35a}$$

where $\alpha_0=(\eta^2-\eta_0^2)^{1/2}$, and is to be considered as

small in comparison with E, F, E', F' which may be taken as constants over each loop. For the loop about η_0, η may be replaced by $\eta_0 - i\theta$ and then α_0 takes the form $\alpha_0 \cong (2v_1/v_0\theta)^{1/2} e^{-\pi i/4}$. Further, as the branch point η_0 is encircled E, F, E', F', are approximately constant while α_0 changes sign.[7] Putting in specifically $\eta = v_1/v_0 - i\theta$, going to large ρ, and replacing $H_0^{(2)}$ by its asymptotic expansion, we find that to the lowest power of $1/\rho$:

$$\Phi_r = \Phi_{r_1} + \Phi_{r_2} + \Phi_{r_3} + \Phi_{r_4} + T_1, \tag{36}$$

where:

$$\Phi_{r_1} = \left[iv_1^2(F'E - FE')/\omega\rho^2(v_1^2 - \bar{v}_1^2)^{1/2}E'^2 \right] e^{-i\omega\rho/\bar{v}_1 - (\omega/v_1)(v_1^2/\bar{v}_1^2 - 1)^{1/2}(h+z)}, \tag{36a}$$[8]

$$\Phi_{r_2} = -(E/\rho E')e^{-i\omega\rho/v_1 - i\omega(h+z)^2/2v_1\rho}, \tag{36b}$$

$$\Phi_{r_3} = \left[v_1^2(F'E - FE')/\omega\rho^2(\bar{v}_2^2 - v_1^2)^{1/2}E'^2 \right] e^{-i\omega\rho/\bar{v}_2 - (i\omega/v_1)(1 - v_1^2/\bar{v}_2^2)^{1/2}(h+z)}, \tag{36c}$$

$$\Phi_{r_4} = \left[v_1^2(F'E - FE')/\omega\rho^2(v_2^2 - v_1^2)^{1/2}E'^2 \right] e^{-i\omega\rho/v_2 - (i\omega/v_1)(1 - v_1^2/v_2^2)^{1/2}(h+z)}, \tag{36e}$$

$$T = i(2\pi\omega/v_1\rho\eta_0)^{1/2}\left[N(\eta_0)e^{-(\omega/v_1)(z+h)(\eta_0^2 - 1)^{1/2}} e^{\pm i(\omega\rho\eta_0/v_1 - \pi/4)} \right]/\Delta'(\eta_0). \tag{36f}$$

where N is the numerator of $A_1(\eta)$, except for $e^{-\alpha_1 h}$, and η_0 represents the position of a pole A_1. The upper or lower signs are to be used as η_0 is above or below the real axis. The F, E, F', E' for the different Φ_r are of course different and may be found from Eqs. (34a) and (34b).

On recalling the discussion of Eqs. (18), the following geometrical interpretation of $\Phi_{r_1} \cdots T$ may be readily verified. The wave Φ_{r_1} will arrive at (ρ, z), according to Eq. (36a), at a time:

$$t(\Phi_{r_1}) = \rho/\bar{v}_1 \tag{37}$$

after the incident wave has been started at $(0, h)$. It is, however, a wave damped with respect to its distance from the interface and the distance of the source from the interface. It must therefore be excited at and travel along the interface. It is apparently excited initially by a direct longitudinal wave to the interface, travels along the upper part of the interface as a transverse wave and excites vertically projected and damped longitudinal waves. This history of Φ_{r_1} would imply that its time of arrival would be

$$t = (h+z)/v_1 + \rho/\bar{v}_1 \tag{37a}$$

rather than that given by Eq. (37). But since it has already been assumed that ρ is large and the velocity contrasts are high it is seen that Eq. (37) may well be taken as the approximation to Eq. (37a) in which the term $[(h+z)/\rho]\bar{v}_1/v_1$ has been dropped because it is small compared to unity.

Φ_{r_2} is simply the directly reflected longitudinal wave and gives nothing new. Its time of arrival is:

$$t = (\Phi_{r_2}) = (\rho^2 + (h+z)^2)^{1/2}/v_1. \tag{38}$$

Φ_{r_3}, however, is also a new wave. Its time of arrival corresponds to paths in the upper medium, at the angle of total reflection for the refracted transverse waves, which are joined by a path on the under side of the interface traversed with the *transverse* velocity of the lower medium. Φ_{r_3}, itself, of course refers to the wave that is observed at (ρ, z). Its origin is apparently the cone in the incident wave that travels at the angle of total reflection for the refracted transverse waves. The next stage in its history (as suggested by its time of arrival and angle of emergence into the second medium) corresponds to the "totally refracted" transverse wave excited by the incident wave and which travels along the under side of the interface. And this finally is partially transformed into the longitudinal waves Φ_{r_3} reemerging from the interface at the same angle as the original exciting wave. That this angle of emergence really corresponds to that of total reflection, θ_{lt}, between the longitudinal waves and refracted transverse waves, readily follows from the fact that by Eq. (36c)

$$q_{r_3}/w_{r_3} = v_1/\bar{v}_2(1 - v_1^2/\bar{v}_2^2)^{1/2} = \tan\theta_{lt}.$$

[7] It may also be noted that E, F, E', F' are all proportional to ω^6 so that except for $e^{-\alpha_1 h}$, $A_1(\eta)$ is independent of ω.

[8] When ω has a negative real part, the conjugates of the above Φ_r should be used, except that factors as $e^{-\omega y}$ must be replaced by $e^{\omega y}$. These changes, though fairly obvious from general physical considerations may be derived rigorously by beginning with an incident wave as Eq. (12) with ω negative, putting the indentation in Eq. (12a) *above* the real axis and evaluating the loops which are drawn in the *first* quadrant.

The time of arrival of this wave is:

$$t(\Phi_{r_3})=\rho/\bar{v}_2+[(h+z)/v_1](1-v_1^2/\bar{v}_2^2)^{1/2}. \quad (39)$$

And again, Φ_{r_4} is the "refracted" wave that appeared in the simpler case of the purely compressional wave system. It behaves as if it travels in the second medium just below the interface with the *longitudinal* velocity in the second medium and travels in the first medium at the angle of total reflection between incident and refracted longitudinal waves, θ_{ll}. Its time of arrival is given by:

$$t(\Phi_{r_4})=\rho/v_2+[(h+z)v_1](1-v_1^2/v_2^2)^{1/2}. \quad (40)$$

T_1, if it exists, is a real surface wave provided the imaginary part of η_0 is small. For then it will decrease essentially as $1/\rho^{1/2}$ which is the mode of decrease for a surface wave. It travels along the upper side of the interface with an effective radial velocity equal to the longitudinal velocity in the first medium divided by the real part of η_0. A diagrammatic representation of these waves is given in Fig. 5.[9]

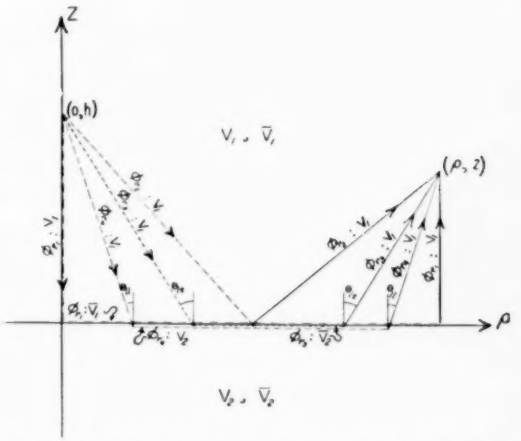

FIG. 5. Geometrical representation of the longitudinal waves excited by an incident spherical longitudinal pulse. Φ_{r_1}: damped wave; Φ_{r_2}: directly reflected wave; Φ_{r_3}, Φ_{r_4}: "refracted" waves. θ_{ll}, θ_{lt} are angles of total reflection. v, $\bar{v}$ are longitudinal and transverse wave velocities.

These waves all refer to the dilatational or longitudinal components of the disturbances excited by the incident longitudinal wave. In addition there are of course similar transverse components represented by the functions χ. Without repeating again the details χ_1 may be represented as the sum of the following functions:

$$\chi_{r_1}=(i\omega E/E'^2\rho^2\bar{v}_1)(E'z+v_1F'/\omega)\, e^{-i\omega\rho/\bar{v}_1-i\omega z^2/2\bar{v}_1\rho-(\omega h/v_1)(v_1^2/\bar{v}_1^2-1)^{1/2}}, \quad (41)$$

$$\chi_{r_2}=(i\omega F/E'^2\rho^2 v_1)(E'h+v_1F'/\omega)\, e^{-i\omega\rho/v_1-i\omega h^2/2v_1\rho-(i\omega z/v_1)(v_1^2/\bar{v}_1^2-1)^{1/2}}, \quad (41a)$$

$$\chi_{r_3}=[iv_1(F'E-FE')/\bar{v}_2\rho^2E'^2]\, e^{-i\omega\rho/\bar{v}_2-(i\omega h/v_1)(1-v_1^2/\bar{v}_2^2)^{1/2}(i\omega z/\bar{v}_1)(1-\bar{v}_1^2/\bar{v}_2^2)^{1/2}}, \quad (41b)$$

$$\chi_{r_4}=[iv_1(F'E-FE')/v_2\rho^2E'^2]\, e^{-i\omega\rho/v_2-(i\omega h/v_1)(1-v_1^2/v_2^2)^{1/2}(i\omega z/\bar{v}_1)(1-\bar{v}_1^2/v_2^2)^{1/2}}, \quad (41c)$$

$$T=i(2\pi\omega/v_1\rho\eta_0)^{1/2}[N(\eta_0)/\Delta'(\eta_0)]\, e^{-(\omega h/v_1)(\eta_0^2-1)^{1/2}-(\omega z/v_1)(\eta_0^2-v_1^2/\bar{v}_1^2)^{1/2}}e^{\pm i(\omega\rho\eta_0/v_1-\pi/4)}, \quad (41d)$$

where in the expressions for χ_r the E and F are to be taken from the coefficient of α_1 in Eq. (34c), so that E, F, $\sim\omega^4/v_1^4$ and E', $F'\sim\omega^6v_1^6$.

The geometrical interpretation of these is the following. χ_{r_1} is a transverse wave that has been apparently excited at the point on the interface that is just below the source. The time of arrival for χ_{r_1}, according to Eq. (41), simply includes the time of transit after excitation,

$$t(\chi_{r_1})=(\rho^2+z^2)^{\frac{1}{2}}/\bar{v}_1, \quad (42)$$

but lacks the term h/v_1 that would be required for the incident wave to reach the point of apparent excitation. This, however, seems to be due to an implicit approximation in which this term, h/v_1, is neglected, since if it were large the exponential damping factor $e^{(-\omega h/v_1)(v_1^2/\bar{v}_1^2-1)^{\frac{1}{2}}}$ would anyway practically extinguish the wave.

χ_{r_2} appears to be a transverse wave that has been excited by a direct longitudinal wave at the point (0, ρ). From Eq. (41a) it would seem that it travels upwards from its point of excitation on the interface, at an angle with the vertical of $\theta=\tan^{-1}1/(v_1/\bar{v}_1^2-1)^{1/2}$. But since, as already mentioned it is implicitly assumed in the analysis that the velocity contrasts are all large, the above angle is the corresponding approximation

[9] When synthesized into pulses Φ_{r_2} will have the same form as Φ_0 Φ_{r_3} and Φ_{r_4} pulses, however, will be distorted in such a way that the velocities and accelerations of Φ_{r_3} and Φ_{r_4} will respectively have the same forms as those of the displacements and velocities of Φ_0.

to a vanishing angle. Its time of arrival is:

$$t(\chi_{r_3})=\frac{(\rho^2+h^2)^{1/2}}{v_1}+\frac{z(1-\bar{v}_1^2/v_1^2)^{1/2}}{\bar{v}_1}$$
$$\leqq\frac{(\rho^2+h^2)^{1/2}}{v_1}+\frac{z}{\bar{v}_1}. \quad (43)$$

χ_{r_3} is again a "refracted" wave. It appears to be excited by the incident longitudinal cone[10] coming at the angle, θ_{lt}, of total reflection between longitudinal and transverse waves; it then travels on the lower side of the interface as a transverse wave and then reemerges as a transverse wave at the angle of total reflection between transverse waves, θ_{tt}. Thus its time of arrival is given by:

$$t(\chi_{r_3})=(\rho/\bar{v}_2)+(h/v_1)(1-v_1^2/\bar{v}_2^2)^{1/2}$$
$$+(z/\bar{v}_1)(1-\bar{v}_1^2/\bar{v}_2^2)^{1/2}. \quad (44)$$

Finally, χ_{r_4} is another "refracted" wave whose exciting cone is incident at the interface at the angle of total reflection between longitudinal waves, θ_{ll}. Its immediate source is the "totally refracted" longitudinal wave which travels on the underneath side of the interface and excites χ_{r_4} as a transverse wave travelling at the angle of total reflection between a transverse and longitudinal wave, θ_{lt}. Its time of arrival is:

$$t(\chi_{r_4})=(\rho/v_2)+(h/v_1)(1-v_1^2/v_2^2)^{1/2}$$
$$+(z/\bar{v}_1)(1-\bar{v}_1^2/v_2^2)^{1/2}. \quad (45)$$

T is again a surface wave and of no immediate interest.

The waves χ_r are represented diagrammatically in Fig. 6. It should be pointed out, however, that only the solid parts of the paths, or those parts for which ρ is large, are definitely indicated by the above analysis. For the angle with the vertical of the direction of propagation of the waves χ_r are given by $\theta=\tan^{-1} w/q$ (for the Φ_r waves $\theta=\tan^{-1} q/w$) and since the expressions for χ_r of Eqs. (41) to (41d) refer to large ρ, the corresponding angles θ will also refer to the regions of large ρ. However, the times of arrival as given by Eqs. (42) to (45) indicate what are at least equivalent geometrical representations of the paths which are finally completed by those portions represented by the analytical expressions for the χ_r. These dotted portions, therefore, do not necessarily represent the analytic continuations of Eqs. (41) to (41c) for smaller values of ρ but rather the probable preliminary longitudinal or transverse waves which finally excited the χ_r waves represented by the solid lines or by the expressions of Eqs. (41) to (41c). The same remarks apply, of course, to the paths indicated in Fig. 5.

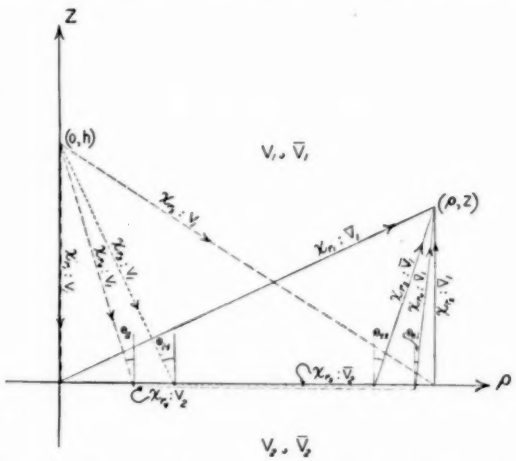

FIG. 6. Geometrical representation of the transverse waves excited by an incident longitudinal pulse. χ_{r_1}: damped wave: χ_{r_2}: reflected wave. χ_{r_3}, χ_{r_4}: "refracted" waves, θ_{ll}, θ_{lt}, θ_{tt}, θ_{tl}, are angles of total reflection. v, $\bar{v}$ are longitudinal and transverse wave velocities.

It may also be of interest to note that the paths of Figs. 5 and 6 are actually minimal time paths from the point of view of geometrical optics. Thus by the method indicated on p. 15, it may be readily verified that by minimizing general paths of the types of Figs. 5 and 6 not only will the angles come out to be the various angles of total reflection given by the above equations of the wave theory analysis, but the minimal times will also coincide with those given in the above equations.

Since the times of arrivals for the above waves are different the resultant wave system at the point of observation (ρ, z) will not be a simple superposition of all the waves recorded at the same instant. Rather, if ρ is sufficiently large and the velocity contrasts are relatively high a single longitudinal pulse originating at the point

[10] This is the same "wave cone" that excites the Φ_{r_3} wave. Similarly, the χ_{r_4} and Φ_{r_4} waves are excited, from a geometrical point of view, by the same incident "wave cone," as may be seen by comparing Figs. 5 and 6.

$(0, h)$ will lead to a series of pulses in the order of the times of arrival given in the above equations. Since:

$$t(\Phi_{r_4}) < t(\chi_{r_4}) < t(\Phi_{r_3}) < t(\chi_{r_3}) < t_d < t(\Phi_{r_2}) < t(\chi_{r_2}) < t(\Phi_{r_1}) < t(\chi_{r_1}) \quad (46)$$

the pulses will arrive at a given point in the order of the arguments of the above inequality. t_d is the time for the direct incident pulse and is evidently equal to $(\rho^2+(h-z)^{1/2}/v_1$.

Of course, after the passage of any particular pulse, the disturbances will not suddenly vanish so that in an actual observation it may be difficult or impossible to distinguish them. But theoretically new impulses should be observed at each of the instants indicated by the above values of t. The strengths of these impulses will also be variable and some may be too weak to be observable. These details as well as the shapes of the pulses can, if desired, be determined from the equations already given.[11] Here, we are concerned mainly with the fact that the refraction paths are *real* and that the displacement components are generally of the order of $1/\rho^2$ and hence may under the proper conditions carry quite appreciable amounts of energy.

Finally it may be noted that the above wave theory analysis shows that when the incident wave is transverse, a similar series of refracted rays will arise. Those that really have refraction characteristics as Φ_{r_3}, Φ_{r_4}, χ_{r_3}, χ_{r_4} of Figs. 5 and 6, are shown in Fig. 7. The times of first arrival are:

$$\left.\begin{aligned} t(\Phi_1) &= \frac{\rho}{v_2} + \frac{h}{\bar{v}_1}(1-\bar{v}_1^2/v_2^2)^{1/2} + \frac{z}{v_1}(1-v_1^2/v_2^2)^{1/2}, \\ t(\Phi_2) &= \frac{\rho}{\bar{v}_2} + \frac{h}{\bar{v}_1}(1-\bar{v}_1^2/\bar{v}_2^2)^{1/2} + \frac{z}{v_1}(1-v_1^2/\bar{v}_2^2)^{1/2}, \\ t(\chi_1) &= \rho/v_2 + [(h+z)/\bar{v}_1](1-\bar{v}_1^2/v_2^2)^{1/2}, \\ t(\chi_2) &= \rho/\bar{v}_2 + [(h+z)/\bar{v}_1](1-\bar{v}_1^2/\bar{v}_2^2)^{1/2}, \end{aligned}\right\} \quad (47)$$

with

$$t(\Phi_1) < t(\chi_1) < t(\Phi_2) < t(\chi_2). \quad (47a)$$

[11] It may be mentioned, however, that when synthesized into pulses the real "refraction" waves χ_{r_3} and χ_{r_4}, just as the Φ_r waves, will have the same velocity and acceleration distributions respectively as the displacement and velocity distribution in the incident Φ_0 pulses.

It may be observed that if $h=z$ and ρ is very large the above waves have the same times of arrival as those for the incidence on the interface of a longitudinal wave. Thus we have:

$$\left.\begin{aligned} &t(\Phi_1) = t(\chi_{r_4}); \quad t(\Phi_2) = t(\chi_{r_3}) \\ \text{and} \quad &t(\chi_1) \leqq t(\Phi_{r_4}); \quad t(\chi_2) \leqq t(\Phi_{r_3}). \end{aligned}\right\} \quad (48)$$

To be certain, therefore, of the nature of the incident wave, it would be necessary, if the question arises, to determine if the *recorded* wave is itself longitudinal or transverse. Thus if a longitudinal wave has been found to arrive at the time corresponding to $t(\chi_{r_4})$, Eq. (48) shows

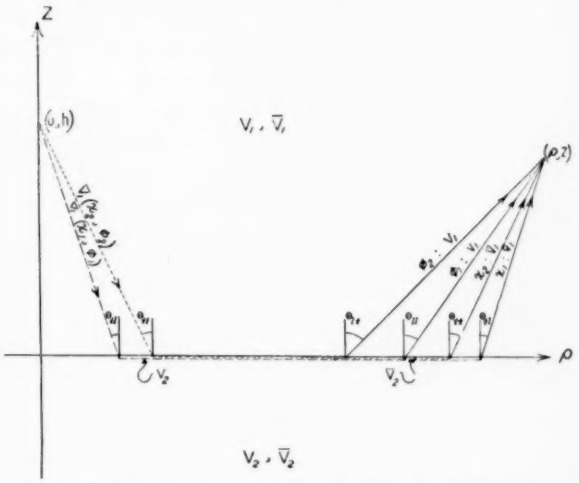

FIG. 7. Geometrical representation of the "refracted" longitudinal (Φ) and transverse (χ) waves excited by an incident transverse wave. θ_{ll}, θ_{lt}, θ_{tl}, θ_{tt} are angles of total reflection. v, $\bar{v}$ are longitudinal and transverse wave velocities.

that it must be the Φ_1 wave resulting from the incidence of a transverse wave pulse, rather than the χ_{r_4} wave excited by the incidence of a longitudinal wave.

Aside from the significance of these results in the theory of refraction shooting it may be of interest to observe that they also suggest an explanation for the apparent velocity contrast that has been reported in the literature[12] between wave velocities parallel and perpendicular to the bedding planes. Thus, rocks or sands which show marked "bedding planes" may be considered as composed of stratified layers each essentially isotropic, but varying among themselves in their wave velocities. Now the analysis developed

[12] B. McCollum and F. A. Snell, Physics **2**, 174 (1932).

above shows that when a high velocity medium bounds one of lower velocity, waves originating in the latter will be refracted into the high velocity medium and effectively travel in it along an interface. This will evidently remain true if the high velocity medium is bounded again by a low velocity layer unless the wave-length of the wave is much larger than the thickness of the high velocity stratum. And since in explosion waves many frequencies are present it does not seem unreasonable that at least some of the energy would effectively travel mainly in the high velocity strata and give rise to an apparent uniform high velocity, parallel to the bedding plane. Across the bedding plane, the thin streaks of high velocity would have an effect proportional only to their total thickness and the average would be approximately the low velocity of the thicker layers of the medium.

One may therefore still retain the assumption of isotropy with regard to the individual strata and attribute the apparent anisotropy to the high velocity refracted rays that will arrive first at the recorder, even if the source be placed in one of the lower velocity strata.

Returning now to the general theory of refraction shooting it may be concluded that the "refraction" paths usually assumed in geophysical analyses are not only geometrically necessary from the point of view of the observed time distance curves, but are in fact a natural accompaniment of the wave interference phenomena arising from the reflection of spherical elastic waves from interfaces between media of different elastic constants.

The writer is indebted to Mr. R. D. Wyckoff and to Drs. L. J. Peters, E. A. Eckhardt and P. D. Foote for helpful discussion and criticism.

A Study of the Electrical Breakdown of Liquids by Means of the Electro-Optical Shutter

HAROLD W. WASHBURN, *University of California, Berkeley*

(Received September 12, 1932)

The static and the impulse breakdown of paraffin oil and xylol were investigated by means of the electro-optical shutter. To obtain satisfactory operation of the shutter it was found necessary to use a double shutter consisting of three crossed nicol prisms and two Kerr cells. Because of the liquids being only commercially pure and of the occluded air and moisture, several types of sparks were observed for a given method of applying the voltage. For the early stages of static breakdown, however, the ionization was usually more intense at the anode. With impulse breakdown in paraffin oil there was observed no increase in uniformity of type of breakdown as compared to static breakdown. With xylol, on the other hand, a fair degree of uniformity in type was observed. This uniformity was due to the extremely short time of voltage application, thus causing a decrease in the secondary effects resulting from impurities and occluded gasses.

INTRODUCTION

THE study of electrical breakdown in liquids has been an object of increasing interest for the past several years. Undoubtedly the extensive use of oil for insulating and for quenching sparks has fostered a good deal of this interest. In spite of the fact that there has been considerable study and experimentation along this line there is very little known about the mechanism of breakdown in liquids. This is probably due to the complicated nature of the breakdown and still more to the extremely short times in which it takes place. In the electro-optical shutter we find an apparatus that is capable of operating in the extremely short time intervals required. That is, with this shutter it is possible to observe the spark in its initial stages of formation. By means of such observations on sparks in air F. Dunnington has been able to determine the initial regions of ionization and how they progress.[1] From these data he has been able to learn something about the space charges. With this shutter Dunnington was also able to determine the rate of fall of voltage across the gap when a spark occurs. Observations are now in progress to determine the spectrum of the light emitted by the initial stages of breakdown. From these data it is hoped to determine the kind of ions that are being formed. It is seen from this that the electro-optical shutter has already proven itself a powerful tool in the study of electrical breakdown.

In the present paper there are presented the first results that have been obtained with the shutter for the breakdown of liquids. In these experiments two methods of applying the voltage were used. (1) The voltage was raised to its maximum value in about one-half second and then held there until breakdown occurred. This will be called static breakdown. (2) The voltage was applied only for 0.3×10^{-6} second. The breakdown resulting from this second method will be called impulse breakdown. Observations of both static and impulse breakdown were made on paraffin oil and on xylol. As would be expected a manner of formation was observed which is decidedly different from that of the "ionization breakdowns" observed in air.

THE ELECTRO-OPTICAL SHUTTER

In developing the electro-optical shutter for use in the study of electrical breakdown of liquids the writer first attempted to use the simple type (see Fig. 1) that was employed successfully by F. Dunnington in the study of sparks in air. This simple shutter was however

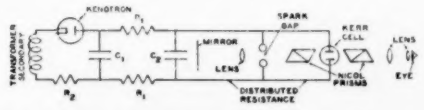

FIG. 1. Diagram of the electrical and optical circuits of the single electro-optical shutter.

[1] Frank G. Dunnington, Phys. Rev. **38**, 1506 (1931).

found to be unsatisfactory for sparks in liquids. That is, the shutter would not close effectively enough to shut out the bright light emitted by the later stages of the spark. To eliminate this difficulty a double shutter was tried which proved to operate satisfactorily. (See Fig. 2.)

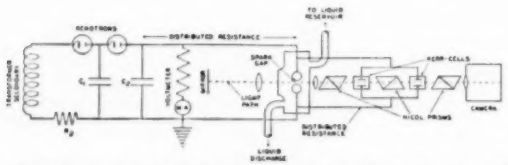

FIG. 2. Diagram of the electrical and optical circuits of the double electro-optical shutter.

In order to make clear the reasons for the improvement of the double shutter over the single shutter it will first be necessary to point out the characteristics of the electro-optical shutter. The operating characteristics of the simple shutter have been fully discussed in a previous paper,[2] and so will only be briefly given here. A diagram of the shutter is shown in Fig. 1. It will be noted that there is an optical system and an electrical circuit. The optical system is composed of two nicol prisms, a Kerr cell, a mirror and lenses. The two nicol prisms are crossed so that no light from the spark passes through them when the Kerr cell is disconnected. The Kerr cell is oriented so that the direction of its electrical field is at 45 degrees to the plane of polarization of the light passed by the first nicol prism. With this arrangement the light from the spark can pass through the shutter only when a voltage is on the Kerr cell. The transmission of the shutter as a function of the voltage on the Kerr cell is shown in Fig. 3. In this diagram 100 percent voltage is the voltage at which the shutter has its maximum opening.

In the electrical circuit R_1 is a resistance of about 10^4 ohms and serves to limit the rate of the building up of voltage on C_2 and hence the spark gap. The distributed resistance between C_2 and the spark gap is 200 ohms which is large enough to make the discharge of C_2 (560 m.m.f.) into the spark aperiodic. The distributed resistance between the spark gap and Kerr cell is adjusted to give the best operating conditions of the shutter. This best value is determined experimentally, as will be described presently.

[2] H. W. Washburn, Phys. Rev. **39**, 688 (1932).

The operation of the shutter will now be briefly described. The voltage on the spark gap is brought up in about one-half second. This voltage is of course also on the Kerr cell and the shutter is therefore open. There is, however, no light passing through the shutter until the spark begins to form. At the instant the spark begins to form the voltage drops across the gap. Because of this drop in voltage the Kerr cell begins to discharge. When it has discharged to an extent which makes the light transmitted by the shutter too feeble to be observed, the shutter is effectively closed. Consequently the light from the spark which is observed is that which passes through the Kerr cell up to the time at which the shutter effectively closes. The stage of development that is observed can be altered either by changing the rate of discharge of the Kerr cell by appropriate changes in the Kerr cell leads or by changing the length of light path between the gap and the shutter. This change in light path can be conveniently obtained by means of a mirror and lens as shown in Figs. 1 and 2. In making observations on sparks in liquids this change in length of light path was accomplished by two 45

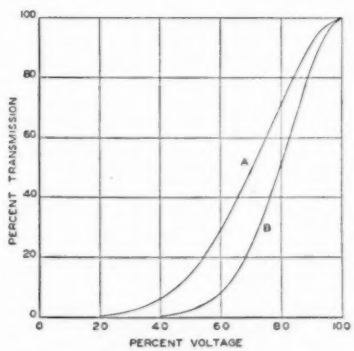

FIG. 3. Light transmission curves. *A*, Single shutter. *B*, Double shutter.

degree mirrors which sent the light back a little to one side of the spark chamber. This was done to avoid unnecessary distortion of the image which would result from again passing the light through the imperfect lens surface formed by the plane windows and adjacent liquid in the spark chamber.

The problem of adjusting the Kerr cell spark gap circuit for satisfactory operation is not as simple as it first appears. It is not only necessary that the Kerr cell discharge rapidly enough but

also that it remain nearly discharged until the spark is quenched. The Kerr cell leads have inductance as well as resistance and so the discharge of the Kerr cell is of an oscillatory nature. If the resistance of the Kerr cell leads is too small the oscillations of voltage on the cell will be large enough to effectively re-open the shutter. If this resistance is too large the Kerr cell will discharge too slowly and the closing time of the shutter will not be short in comparison with the formation time of the spark. Both of these effects pass light from the later stages of the spark and so it is not a difficult matter experimentally to determine the resistance which gives the most satisfactory operation of the shutter.

Although it was possible to obtain good results with this simple shutter for sparks in air it was not found possible to obtain satisfactory operation for sparks in paraffin oil or xylol. No resistance could be found which would not pass so much light from the later stages of the spark that the earlier stages were either masked or obliterated. This was probably due either to the later stages of the sparks in liquids being so much brighter than earlier stages, or to a relatively high voltage appearing across the gap after the spark had formed. Using the cathode-ray oscillograph, Rogowski has observed that in oil the voltage may return to a considerable value (about 1 kv for a 0.15 mm gap) in about 10^{-6} seconds after the first major drop at the beginning of breakdown.[3]

By employing a double shutter as shown in Fig. 2, both of the above-mentioned difficulties can be overcome. The double shutter consists essentially of two single shutters optically in series and electrically in parallel. The second nicol prism is crossed with the first and the third with the second. Both Kerr cells are oriented so that their electrical field is at an angle of 45 degrees to the plane of polarization of the incident light. The transmission curve of this double shutter is shown in Fig. 3. It is obtained by squaring the ordinates of the transmission curve for the single shutter. It will be noted that the double shutter has the same transmission at 100 percent voltage but that its transmission for the lower voltages is considerably lower than that of the single shutter. As regards the rapidity of closing of the double shutter it is seen that its transmission falls more rapidly with voltage. On the other hand the rate at which the voltage drops is reduced since the Kerr cell capacity has been doubled. Calculations show that these two factors just about neutralize each other. Consequently the rate of closing of the two shutters is approximately the same. The double shutter, however, has the disadvantage of having a much longer light path which reduces the amount of light that can be collected from the spark and passed through to the observer. The double shutter would therefore be used only where a more complete closing is necessary to prevent the passage of light from the later stages of the spark.

[3] W. Rogowski, Arch. f. Elektrotechnik **18**, 510 (1927).

The Electrical Breakdown of Liquids

Results of other experiments[4, 5, 6] on the breakdown of liquid dielectrics have shown that the breakdown voltage for a given temperature and pressure varies considerably with the duration of the application of voltage and with the purity and gas content of the liquid. Nikuradse points out that, with transformer oil which has been carefully purified and outgassed, the breakdown voltage is extremely high, being of the order of 1.3×10^{6} volts per centimeter. Experiments on thin films indicate that the breakdown in pure outgassed oil is a pure "ionization" breakdown.[7] A pure ionization breakdown is conceived as an ionization by collision process that results from the destruction of the dielectric properties of the liquid as distinguished from the destruction of these properties by secondary effects such as ionizations caused by the presence of impurities, occluded air or moisture, or by a temperature rise resulting from the conduction current. In the article just referred to Nikuradse also shows that, as the time of voltage application decreases, the breakdown voltage increases and the secondary processes have less effect. For an impulse voltage as short as 10^{-9} to 10^{-10} second he shows that the secondary effects would have completely

[4] A. Nikuradse, Arch. f. Elektrotechnik **25**, 826 (1931).
[5] L. Inge and A. Walther, Arch. f. Elektrotechnik **23**, 279 (1930).
[6] H. Edler, Arch. f. Elektrotechnik **25**, 447 (1931).
[7] A. Joffe, Zeits. Sowj. **1**, 255 (1932).

vanished and that in all probability a pure ionization breakdown would be obtained.

From the above discussion it appears that one should start experimenting with a pure outgassed liquid, since the pure ionization breakdown is much simpler than the breakdowns resulting from many secondary effects. With the simpler phenomenon one would have a better chance of unravelling the mechanism. On the other hand, a single breakdown in the pure outgassed liquid so changes its properties that subsequent breakdowns occur at a much lower voltage. This means, of course, that only one observation can be made with each sample that is prepared. Since in the present experiment the electro-optical shutter was being developed for use with breakdown in liquids and since this development required hundreds of observations, it was not practical to start with pure liquids. With the knowledge gained from the present experimentation, however, it is believed that it will not be difficult to obtain observations on pure liquids. This is to be the next experimental study by the writer.

In the present study observations were taken on commercially pure paraffin oil and xylol both for static breakdown and an impulse breakdown of 0.3×10^{-6} second. It was necessary to use an impulse voltage as long as this since it takes between 10^{-8} and 10^{-7} second to charge up the Kerr cells. This will be made clear in the discussion of the impulse circuit which will be given in the next section of this article. The results obtained with paraffin oil and impulse breakdown were nearly as complex as those obtained with static breakdown. On the other hand the impulse breakdown of xylol gave much more uniform results than were obtained with static breakdown.

The Impulse Circuit

The impulse circuit employed makes use of the usual scheme of initiating the impulse by means of a secondary spark gap. The circuits ordinarily employed, however, were not directly applicable as they require a very small capacity of the gap to which the impulse is applied. In our case the Kerr cells are connected across this gap and a small capacity is therefore not realized. An additional difficulty is that the spark gap-Kerr cell circuit is oscillatory. It is desirable that the impulse voltage be applied in such a way that the Kerr cells and spark gap come up to a given voltage and then remain there. If oscillations occur this condition of course will not be obtained. It was approximately obtained by placing a large resistance between the gap and the supply condenser (R_4 in Fig. 4).

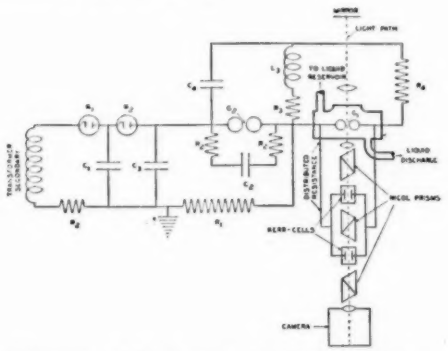

FIG. 4. Diagram of the impulse circuit used in connection with the electro-optical shutter.

The operation of this impulse circuit is made clear by a study of the diagram shown in Fig. 4. The voltage is applied to the transformer which brings up the voltage on G_2, C_2, and C_4 in about one second. This rate of voltage build-up is controlled by the filament current in K_2 and by R_1 which is about two megohms. The voltage is raised until a spark occurs at G_2. This spark may be thought of as suddenly connecting C_4 to the test gap G_1 and Kerr cells through R_4. The resistance R_4 was 200 ohms which is large enough to reduce the oscillations to less than five percent of the voltage on C_4. A larger resistance would make the discharge at G_1 too feeble. The resistances R_2 were 40 ohms apiece which was sufficient to make the spark at G_2 last somewhat longer than 0.3×10^{-6} second. The inductance and resistance L_3 and R_3 were adjusted so as to limit the time to which full voltage was applied to G_1 to about 0.3×10^{-6} second. The calculated test gap voltage-time characteristic is the solid curve shown in Fig. 5. The dotted curve is the breakdown voltage of a 0.8 mm gap in unpurified transformer oil plotted as a function of the time of voltage application. This curve was taken from curves given by R. Naher.[8] It is seen that the voltage-time characteristic of oil is such that

[8] R. Naher, Arch. f. Elektrotechnik **21**, 169 (1929).

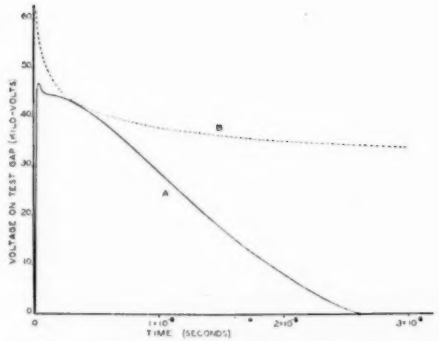

FIG. 5. Curve *A*, calculated impulse voltage applied to test gap. Curve *B*, impulse breakdown voltage characteristic of unpurified transformer oil.

an impulse voltage with a long trailing foot, such as the one shown, can be used without danger of incurring any appreciable variation in the time or the voltage of breakdown.

EXPERIMENTAL PROCEDURE

In taking observations of static breakdown the potential was first adjusted to 45,000 volts. This was the voltage that gave maximum opening of the shutter. The voltmeter used consisted of fifty feet of one-quarter inch glass tubing through which distilled water was circulated. The current taken by this water column was about 100 microamperes at 50,000 volts. There was therefore no appreciable ripple introduced by the voltmeter. The resistance of the water column was determined each day with a 5000 volt (calibrated) electrostatic voltmeter. After the voltage was set, the gap was adjusted until the breakdown occurred in one to ten seconds after the application of voltage. About ten seconds were allowed between each breakdown in order that the gas bubbles formed by the spark could rise out of the field between the electrodes. As was previously stated, liquids of commercial purity were used. With this purity about fifty breakdowns could be observed on the same sample before any noticeable effect on the breakdown voltage occurred. The electrodes, which were eight millimeter brass spheres, were cleaned and polished after every 200 breakdowns. With the small energies of discharge employed there was very little corrosion of the electrodes.

In taking observations of impulse breakdown, the spark gap G_2 was adjusted so that 35,000 volts would occur across the test gap G_1. The test gap electrodes were then set at the maximum spacing at which a spark would occur. The rest of the procedure was similar to that just given for static breakdown.

DETERMINATION OF THE OPEN TIME OF THE SHUTTER

The length of time that the shutter remains open after the beginning of breakdown can be calculated from the circuit constants and a knowledge of the rate at which the gap voltage falls.[2] For our present qualitative study, however, an accurate knowledge of this time is not necessary. Indeed it would be impossible to make an accurate calculation without an accurate knowledge of the rates of voltage drop for our particular conditions. A quantity known as the "path time" will therefore be used as a measure of the open time of the shutter. The path time is defined by the following expression: Path time $= T_w - T_l$, where T_w = length of wire path between the spark gap and Kerr cell divided by the velocity of light; T_l = length of light path between the spark gap and Kerr cell divided by the velocity of light. An inspection of Fig. 2 will show that this path time is the interval of time between the instant at which the light from the beginning of the spark reaches the Kerr cell and the instant at which the beginning of the voltage wave from the spark gap reaches the Kerr cell. The actual open time of this shutter is somewhat longer than the path time.[1, 2] If the time that it takes the voltage to drop for our conditions is 10^{-8} second, about 0.8×10^{-8} second should be added to the path time to obtain the open time of the shutter. This value was obtained by making some calculations for the particular leads used and by assuming the voltage to drop in 10^{-8} second.

EXPERIMENTAL RESULTS

a. Static breakdown of paraffin oil

The observations of the static breakdown of paraffin oil were taken with a potential of 45,000 volts and the gap adjusted for breakdown to occur in from 1 to 10 seconds after the application of voltage. This gap was found to be 2.1 millimeters. Observations of the earliest part of the breakdowns were made visually as the light emitted was too feeble to photograph. With the

shutter set for a path time of -0.8×10^{-8} second no light at all could be seen. This is to be expected since an approximate correction of this path time by the figure given in the preceding section gives zero time. In other words, with this setting, the shutter closes at the instant the spark begins to form. For a setting of -0.6×10^{-8} second path time the spark is visible. Due to the commercial purity of the oil several types of sparks were observed. They all have, however, certain common characteristics, as follows. As soon as the spark is visible at all it is visible throughout the greater part of the distance between the electrodes. Some parts are brighter than others but completely dark spots usually occur singly or in pairs and only cover a relatively small portion of the gap. Occasionally an exception to this rule occurs when the spark begins by emitting light only at several points in a line between the electrodes (No. 7, Fig. 6). Fig. 6 shows a few freehand drawings which were made of each spark at the time of its observation.

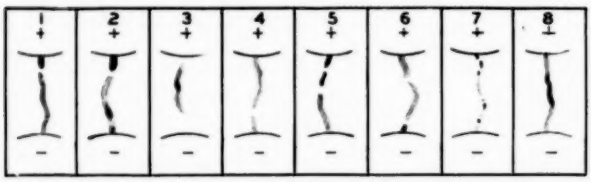

FIG. 6. Freehand drawings of initial stage of static breakdown of paraffin oil. Path time $=-0.6\times10^{-8}$ second.

The manner in which the spark in oil begins differs markedly from that of sparks in air.[9] As was found by Dunnington the sparks in air start by intense ionizations at the electrodes and under certain conditions with an additional region between the electrodes.

For path times of 0.06×10^{-8}, 0.3×10^{-8}, and 0.8×10^{-8} second the light intensity was sufficiently bright to be photographed. A few of the pictures obtained are shown in Fig. 7. The numbers under the sparks indicate the number of times that type of spark occurred out of fifty sparks taken with the same shutter setting. It will be noted that for the shortest path times photographed (0.06×10^{-8} sec.), the sparks having one or two points of intense ionization at the anode occur most frequently (types 1 and 2 in Fig. 7). At the two later times (0.3×10^{-8} and 0.8×10^{-8} sec.) photographed, the predominating sparks are those having either several points of intense ionization or nearly uniform ionization throughout their length. These types are shown in columns 9 to 14 in Fig. 7.

The pictures in the row labeled "no shutter" were taken with the nicol prisms uncrossed and the Kerr cells disconnected. The diaphram in the first lens was cut down so that the brightest parts would give densities well below the saturation point of the plate. These pictures therefore show an integration of the intensities emitted throughout the duration of the entire spark. The length of this time is of the order of magnitude of 10^{-6} second. It is seen that the regions of intense ionization in over half the cases are differently located than in the case of any observed spark at the early stages of breakdown. The most predominate type apparently has its highest intensity at both electrodes. It would be well to mention at this point that the intensities of light emitted by the spark are decidedly not proportional to the density of blackness on the pictures shown. The contrast is exaggerated by the photographic process. This explains why some points occur in the spark, even with no shutter action, that are perfectly white.

b. Impulse breakdown of paraffin oil

In taking observations of the impulse breakdown of paraffin oil the voltage was adjusted to 35,000 and the gap set at the maximum spacing at which a spark would occur. The spacing of the electrodes thus obtained was about 0.4 millimeter. The observations of all the impulse breakdowns were made visually as the images were too weak to photograph. No light from the spark was visible with a path time as short as -0.8×10^{-8} second as was the case with static breakdown. With the shutter set for a path time of -0.4×10^{-8} second a very faint haze is seen between the electrodes. This haze is not uniform but takes various shapes. With a path time of -0.3×10^{-8} second bright spots begin to appear in this haze. These bright spots apparently do not appear in any particular region but occur as often somewhere between the electrodes as at the electrodes. For path times as long as 0.5×10^{-8} second about eight out of ten sparks show nearly uniform ionization throughout their length. Fig. 8 shows some freehand drawings made of these sparks.

[9] F. Dunnington, Phys. Rev. **38**, 1535 (1931).

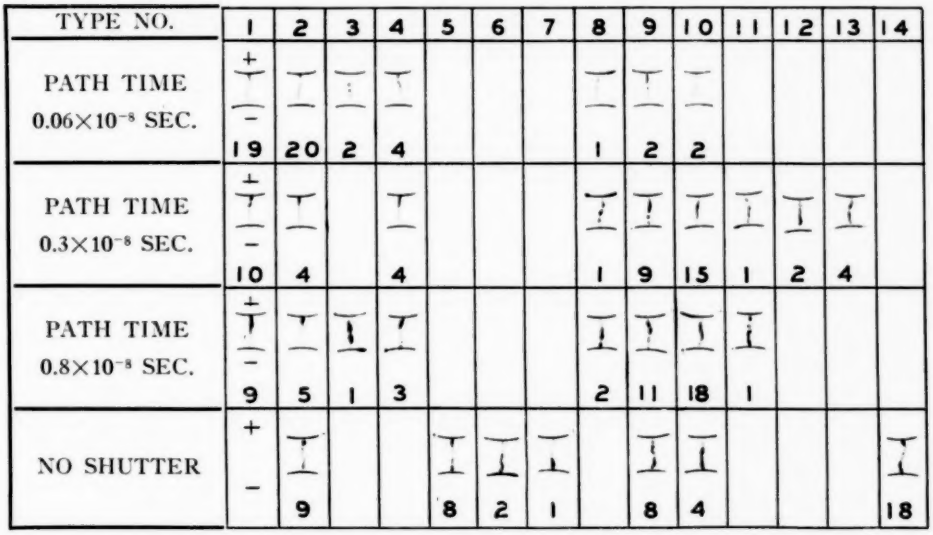

FIG. 7. Photographs of single sparks obtained by the static breakdown of paraffin oil.

It will be noted that, even though the breakdown voltage to impulse potentials for this oil is not far below that of pure outgassed oil, the manner of breaking down is not uniform as would be expected of pure outgassed oil.

c. Static breakdown of xylol

The observations on xylol were made for a potential of 45,000 volts and the gap, adjusted as before, was found to be 2.3 millimeters. With the apparatus adjusted for a path time of -0.8×10^{-8} second nothing could be observed. This agrees with the results obtained with paraffin oil. At a path time of -0.6×10^{-8} second only a very dim haze between the electrodes was visible. At a path time of -0.4×10^{-8} second regions of intense ionization began to appear, usually at the anode. Sometimes the spark would be fairly bright throughout its length. As these observations were all visual it was necessary to record the results by freehand drawings. The types observed at this early time were, however, the same as those recorded photographically at a path time of 0.06×10^{-8} second (see Fig. 9). The drawings are therefore not shown. The essential difference between the beginning of the spark in xylol and in paraffin oil is that the ionization in xylol at first is more localized and larger gaps in the spark appear.

For path times of 0.06×10^{-8}, 0.3×10^{-8}, and 0.8×10^{-8} second the light intensity was bright enough to photograph. The several types of sparks obtained are shown in Fig. 9. As before, the numbers under the pictures indicate the

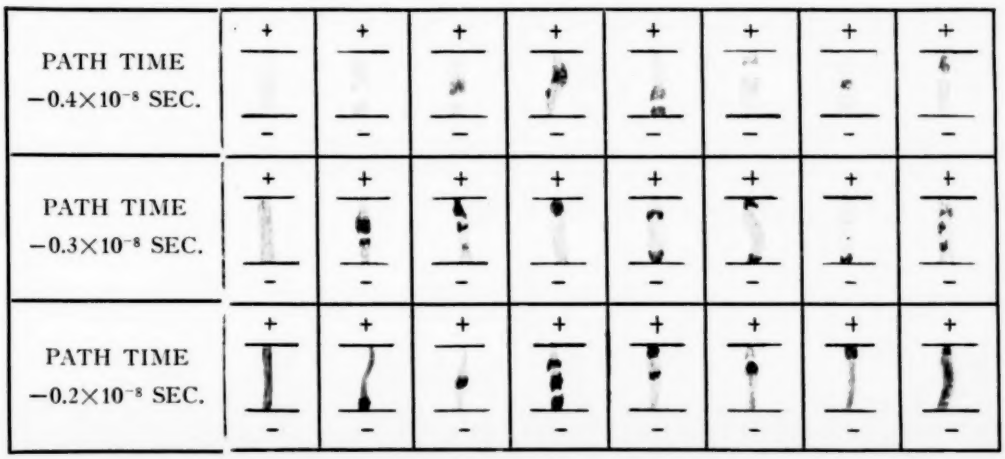

FIG. 8. Freehand drawings of sparks obtained by the impulse breakdown of paraffin oil.

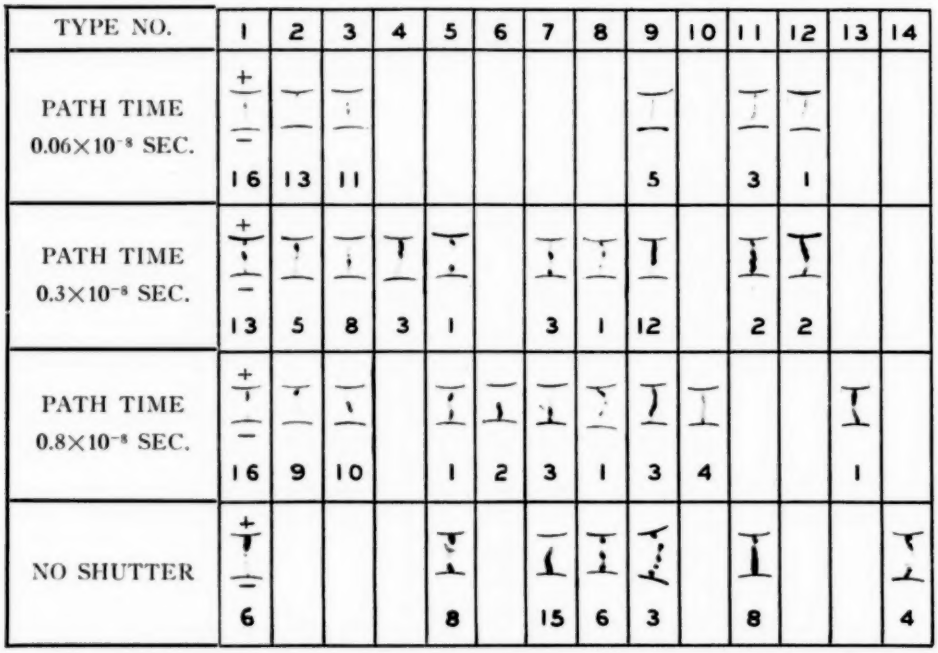

FIG. 9. Photographs of single sparks obtained by the static breakdown of xylol.

number of times that spark occurred out of a group of fifty sparks. It will be noted that for the three path times shown the type of spark occurring most frequently has a single or double region of intense ionization at the anode. It will be recalled that this was the case for the earliest stage photographed with paraffin oil.

The column labeled "no shutter" was obtained in the same way as for paraffin oil. It will be noted that sparks having a double region of intense ionization at the cathode occur twice as often as those having this region at the anode. Another great difference between these sparks and those obtained for the initial stages of breakdown is that sparks having regions of intense ionization at both electrodes are quite numerous whereas for the early stages this type very seldom occurs.

d. Impulse breakdown of xylol

The impulse breakdown of xylol was observed for an applied potential of 35,000 volts. The gap was adjusted as previously described and found to be 0.5 millimeter. Again with the apparatus set for a path time of -0.8×10^{-8} second no light from the spark could be observed. At a path time of -0.3×10^{-8} second the spark appeared as a faint haze between the electrodes and occasionally in addition a bright spot at just one or at both electrodes (see Fig. 10). At a path time of zero seconds the spark was usually fairly bright all the way across with the regions at one or both electrodes brighter, as is shown in Fig. 10. A bright region, however, occurred at the anode more often than it did at the cathode. At a path time of 0.5×10^{-8} second the spark was always bright throughout its length. Sometimes a region brighter than the rest would occur at one or both electrodes but more often at the anode. It is interesting to note here that, with impulse breakdown of commercially pure xylol, fairly uniform results were obtained.

DISCUSSION

From the experimental results just described it is seen that there are several types of sparks which occur in commercially pure paraffin oil and xylol. In fact the results are so complex that it is difficult to draw any definite conclusions as to the mechanism of breakdown. It might be instructive, however, to suggest an explanation for the intense ionization observed at the anode in the early stages of breakdown. From a consideration of the views on cataphoresis of Lenard and of Coehn and from the experiments of Dyk,[10] it is the belief of L. B. Loeb that when liquids, such as

[10] Karl Dyk, Phys. Rev. **31**, 913 (1928).

those studied by the writer, are subjected to a high electric field the gas bubbles present in the liquid will move to the anode. Since in the present experimentation no attempt was made to remove the gas from the liquids, an accumulation of gas bubbles at the anode would be expected soon after each application of voltage. These gas bubbles might be expanded by the heating and consequent evaporation of the surrounding liquid into the bubbles as suggested by Inge and Walther.[5] With a sufficient expansion the breakdown would start by ionization within the bubble. On the other hand the mere accumulation of the gas bubbles at the anode might be sufficient to initiate the breakdown. In either case

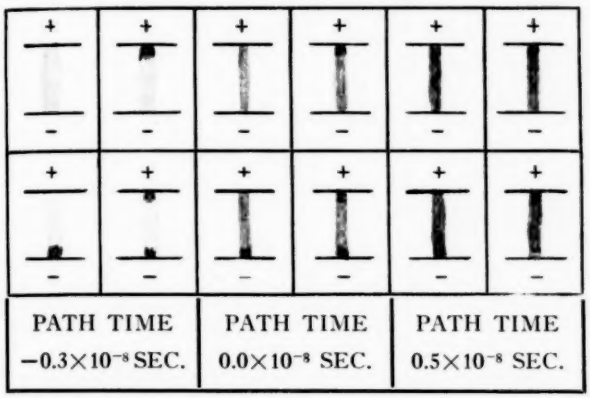

FIG. 10. Freehand drawings of single sparks obtained by the impulse breakdown of xylol.

their presence at the anode would in part account for the intense ionization observed in this region during the early stages of breakdown. It is of interest to note further that the time required to move the bubbles to the electrode would explain the increase in breakdown voltage with the increase in frequency of the applied voltage (in the range zero to 800 cycles) as observed by Draeger.[11]

From the results of impulse breakdown the following observation is of interest. The fact that uniform results were obtained for the impulse breakdown of xylol indicates that the secondary effects have been nearly eliminated by the short time of application of voltage. On the other hand the results for paraffin oil indicate that the secondary effects in its breakdown have not been eliminated. Inge and Walther came to this same conclusion from their experiments. They found that the breakdown voltage of xylol for an impulse of 0.2×10^{-6} second did not vary with pressure, temperature, or occluded air and varied only slightly with impurities. On the other hand the impulse breakdown of transformer oil showed a variation with pressure and temperature. As was previously stated Nikuradse[4] showed that these secondary effects could be eliminated in the breakdown of transformer oil for impulses as short as 10^{-9} to 10^{-10} second.

It should be emphasized that it is very desirable to obtain pictures of sparks in very pure outgassed liquids. When this has been done the effect of impurities and occluded air can be experimentally determined. Such experiments would throw light upon the present results, and a better understanding of the mechanism of breakdown would undoubtedly result. It is hoped that it will be possible in the near future to obtain results along this line.

CONCLUSIONS

(1) In the static breakdown of paraffin oil ionization occurs throughout almost the entire distance between the electrodes in 2×10^{-9} second. This ionization is not uniform but may have one, two, or sometimes several regions of higher intensity. At the earliest time at which the spark can be photographed it was definitely determined that these regions of high intensity usually occur at the anode.

(2) In the static breakdown of xylol the ionization in the initial stages of breakdown is more localized than with paraffin oil. At the earliest time that the spark could be clearly seen ($T_p=-0.4\times10^{-8}$ sec.) the type most often observed had one or two regions of intense ionization at the anode.

(3) By applying an impulse voltage of 0.3×10^{-6} second to paraffin oil no gain in uniformity of the type of spark was obtained.

(4) The results for the impulse breakdown of xylol showed an improvement in uniformity over the static breakdown. The early stages of the spark showed an intense ionization at one or both electrodes.

In conclusion I wish to express my appreciation to Professor E. O. Lawrence for his valuable suggestions and cooperation in carrying out this experimentation.

[11] K. Draeger, Arch. f. Elektrotechnik **13**, 366 (1924).